

Nanocrystal-based optical diffusers for white LED lighting: inverse design achieved by machine learning technologies

by

Gangyi Li

A thesis submitted in partial fulfillment of the requirements for the degree of

Master of Science

in

Microsystems and Nanodevices

Department of Electrical and Computer Engineering
University of Alberta

© Gangyi Li, 2023

Abstract

Illumination receives a great deal of attention as white lighting-emitting diodes (WLEDs) become energy-efficient light sources in households and commercial buildings, on streets and highways, and at stadiums and construction sites. In general, lenses and mirrors are used to control the spatial distribution of WLED light. In this thesis, we propose to use optical diffuser, the key optical device in scattering optics, to achieve the desired figures of merit for WLEDs. Optical diffusers are typically used to create soft light (similar brightness from any angle of view), however, here we can alter the concentration of nanocrystals in the nanocomposite film (optical diffuser) to control its optical property. Machine learning is employed to achieve the inverse design of the optical diffuser pattern on WLEDs, and this design task is beyond human capacities which are generally carried out using the brute force approach (solving a problem through exhaustion). In this thesis work, we have constructed the neural network architectures for machine learning and used them to achieve the inverse design of a symmetric pattern of optical diffusers (two-dimensional design) on WLED modules. Furthermore, we focus on achieving the inverse design of non-symmetric patterns of optical diffusers (three-dimensional design), and several pre-defined patterns of WLED light intensity are demonstrated for showing the success of our efforts.

Preface

This thesis is submitted for the degree of the Master of Science at University of Alberta. This Master thesis contains results of the research undertaken in the Department of Electrical and Computer Engineering, University of Alberta, from September 2021 to December 2022, under the supervision of Professor Xihua Wang and Professor Hao Liang.

Chapter 2 of this thesis is based on a journal publication - Gangyi L, Yuan L, Qiwei X, Hao L, and Xihua W, "Deep learning enabled inverse design of nanocrystal-based optical diffusers for efficient white LED lighting," *Appl. Opt.* 61, 8783-8791 (2022). I was responsible for building optical module and carrying out simulation works with the instructions from Qiwei X. Yuan L led the work on the design and training of neural network models, and I also participated in validation of neural network models. Wang X and Hao L were the corresponding authors.

Chapter 3 of this thesis is based on a paper titled "Scattering optics for LED lighting achieved by nanocrystals and machine learning", and the manuscript is in preparation. I and Yuan L are co-first authors of the paper. My work focused on constructing optical module and carrying out simulation. Yuan L was responsible for designing the entire deep learning approach and training the models. Wang X and Hao L are the corresponding authors.

Acknowledgement

As the farewell for my life at University of Alberta, foremost, I would like to express my deepest respect and thanks to my supervisors, Professor Xihua Wang and Professor Hao Liang, who give me the chance to pursue my Master degree at University of Alberta in Canada. I still could remember scene I met with them at first time, they gave me a lot of advice to help me get used to the new environment and the chances to participate in their research groups. In the past two years, When I encounter difficulties in my research work or taking courses, they will always provide me with patient and excellent guidance and instructions, even sacrificing their rest time. The two professors always give me advice and training on my weakest part communication and presentation skills, which have been really helpful for my job hunting. I do believe what they taught to me and what I learned from them in these two years will be the most valuable fortune for my future work and life.

And I also want to address my sincerest appreciation to all my colleagues: Yuan Liu, Qiwei Xu, Ian Then, Zihan Wang, Jiangwen Zhang. Without their generous support and help, I don't think I can finish all these accomplishments and work just by myself. Every time I encounter difficulties in the road of doing research, you will always give me positive and effective help and support. And thank you for all your care and understanding in the last two years, all these unforgettable memories you leave to me and the friendship we developed will be stored in my mind forever. I with everyone can move forward smoothly in pursuit of the desired goal and finally get the desired outcomes.

At the end, I would like to appreciate all these years' support from my parents, who always stand behind my back and give me everything they have. Also, I want to thank my roommates Shangda Lyu and Zhongyu Zhang, wishing they could have a bright future after graduation.

Thank you for everyone, I love you all. Nevermore.

Table of contents

Chapter 1. Introduction	1
1.1 Introduction to white light-emitting diodes (WLED)	1
1.1.1 What is a WLED	1
1.1.2 Figures of merit of WLEDs	2
1.1.3 Conventional methods to improve the performance of WLEDs	8
1.2 Improving the performance of WLEDs by employing cellulose-nanocrystal (CNC)-based optical diffusers	9
1.2.1 Superior properties of CNC as an optical diffuser on WLED modules	10
1.2.2 Challenges in design related parameters of CNC film pattern	14
1.3 Applying deep learning to the inverse design of optical diffusers for WLED modules	15
1.3.1 What is deep learning	15
1.3.2 Different types of neural networks involved in the research	16
1.4 Objectives and outline of the thesis	18
Reference	20
Chapter 2. Deep learning enabled inverse design of nanocrystal-based optical diffusers for efficient white LED lighting	25
2.1 Introduction	25
2.2 Simulation methods	29
2.2.1 Simulation methods	29
2.2.2 Original data collection	32
2.3 Inverse design methodology	34
2.4 Results and discussion	34
2.4.1 Forward predicting architecture and model evaluation	34
2.4.2 Inverse network design	36
2.4.3 Sampling-based search for the best performances	36
2.5 Conclusion	36
Reference	44
Chapter 3. Scattering optics for LED lighting achieved by nanocrystals and machine learning	48

3.1 Introduction	48
3.2 Experimental Section	51
3.2.1 Optical modeling of WLED coated with CNC nanocomposite films	51
3.2.2 Inverse design of CNC nanocomposite films for desired spatial distribution of LED light intensity	53
3.2.3 Training dataset for machine learning inverse design	56
3.3 Result and Analysis	57
3.3.1 Inverse design: model developed and evaluation	57
3.3.2 Inverse design for user-defined gradually changing patterns	62
3.4 Conclusion	63
Reference.....	65
Chapter 4. Conclusions and future works	67
4.1 Conclusions	67
4.2 Future works	68
4.2.1 Fabrication and experimental verification	68
4.2.2 Improvement of neural network architecture	69
Appendix – Optical simulation using Zemax	70

List of Tables

<i>Table 2-1: Ranges and step sizes of concentration, thickness, angle of coverage, and angle of the ring shape</i>	<i>42</i>
---	-----------

List of Figures

<i>Figure 1-1: (a) The typical structure of WLED. (b) Emission spectrum of the white LED.....</i>	<i>2</i>
<i>Figure 1-2: An example of the spectral radiant flux of a WLED.</i>	<i>3</i>
<i>Figure 1-3: Standard luminous efficiency functions.</i>	<i>4</i>
<i>Figure 1-4: The CIE 1931 chromaticity coordinates.....</i>	<i>6</i>
<i>Figure 1-5: The CIE XYZ standard observer color matching functions.</i>	<i>7</i>
<i>Figure 1-6: Schematic cross-sectional view of (a) dual-layer and (b) conventional remote phosphor structures.</i>	<i>8</i>
<i>Figure 1-7: Schematic diagram of PTFs: (a) red LED, (b) laminated white LED.....</i>	<i>9</i>
<i>Figure 1-8: (a) Picture of CNC nanocomposite film-based optical diffuser with different CNC concentrations (0.5, 1, 2, 4 wt.%) (b) The physical properties of the diffusers withstand the applications of twisting, stretching, and bending. (c) Optical diffusion of a 635 nm laser beam by CNC nanocomposite film-based optical diffusers with different concentrations (wt%) of CNC and compared with market diffusers.</i>	<i>12</i>
<i>Figure 1-9: ACU of a 635 nm laser beam after passing through CNC nanocomposite film-based optical diffuser with different concentrations of CNC: (a) 0.5, (b) 1, (c) 2, and (d) 4 wt%.....</i>	<i>14</i>
<i>Figure 1-10: The schematics of the main neural network architectures in deep learning.....</i>	<i>16</i>
<i>Figure 2-1: (a) Bare WLED packaging module. (b) luminous flux and ACU optimization by coating the WLED module with coverage and a ring shape, where θ is the angle of coverage, and ϕ is the angle of the ring shape. (c) Angular CCT of WLED module with various coverage angles based on ring angle ($\phi=60^\circ$), the concentration of 4 wt.%, and film thickness of 0.3 mm. (d) Luminous flux as a function of angle of coverage.</i>	<i>29</i>
<i>Figure 2-2: Variation of simulated results of Δ CCT (red dashed line) and luminous flux (blue line) according to each parameter: (a) Concentration. Fixed parameters are coverage ($\theta=40^\circ$) and ring ($\phi=70^\circ$) shapes with a thickness of 0.3 mm. (b) Thickness. Fixed parameters are coverage ($\theta=70^\circ$) and ring ($\phi=50^\circ$) shapes with 4 wt.% concentration. (c) The angle of coverage. Fixed parameters are the ring angle ($\phi=65^\circ$) with concentration and thickness of 4 wt.% and 0.3 mm, respectively. (d) The angle of the ring shape. Fixed parameters are the coverage ($\theta=50^\circ$) shape with 4 wt.% concentration and 0.2 mm thickness.</i>	<i>32</i>
<i>Figure 2-3: Flowchart of the entire design scheme using deep learning approach.....</i>	<i>34</i>
<i>Figure 2-4: (a) Forward neural network consisted of fully connected DNN. This forward predicting model takes concentrations, thickness, angle of coverage, and ring shape angle of</i>	

CNC nanocomposite films as inputs and generates luminous flux and Δ CCT. (b) Comparison of simulated (red dotted dashed line) and predicted (blue dotted line) luminous flux and Δ CCT of samples in the normalized training set. The percentage error (green line) is the absolute difference between simulations and predictions in percentage..... 36

Figure 2-5: (a) Inverse predicting tandem architecture formed with DNN-based inverse neural network, nonlinear constraints layer, and pretrained forward DNN model. The inputs and outputs of this network are both luminous flux and Δ CCT. (b) The evaluation of the inverse predicting tandem model for 20 random combinations of the two performances shows the differences between target performance sets (blue line) and verified simulations (red dashed line) based on predicted parameters. 39

Figure 2-6: Workflow of the common method to search the performances. (A) Create diverse sets of structural parameters. (B) Simulate the luminous flux and Δ CCT for each parameter set. (C) Check the simulated results with the required figure-of-merits. This approach needs to iterate these steps before meeting the goals and enormous simulations are time-consuming. 40

Figure 2-7: (a) The performance sets of the original data set used in the forward DNN model. (b) Comparison of the best performance sets in the original data set (red dashed line), improved performance (blue line) predicted from the inverse predicting model, and enhanced performances (green dots) by sampling searching with the forward DNN model. (c) Schematic of sampling-based search using pretrained forward DNN model. (d) Visualization of the structures of CNC nanocomposite layers based on two optimized parameter sets. 43

Figure 3-1: Schematic of spatial light distribution illuminated from CNC nanocomposite film coated WLED module. 49

Figure 3-2: Two iterations of intuitive design “3” shape luminous flux distribution by varying the CNC nanocomposite film blocks corresponding to the previous spatial light intensity distribution.51

Figure 3-3: Flowchart of the entire design scheme of (a) intuitive inverse design. (b) machine learning inverse design. 55

Figure 3-4: The related design and simulated results of shape “3” in both the original data set and predicted by the dee learning method. (a) CNC nanocomposite film concentration distribution in original data set. (b) Simulation result of brightness distribution in the original data set. (c) Concentration distribution predicted by deep learning approach. (d) Verified simulation result of the brightness distribution of neural network architecture. (e) The comparison of the two brightness distributions in the line chart.61

Figure 3-5: (a) The “O” shape as the desired gradually varying light distribution target. (b) The concentration distribution of CNC nanocomposite film and its (c) simulated result of brightness distribution in an intuitive design. (d) The concentration distribution of CNC nanocomposite film and its (e) simulated result of brightness distribution in machine learning design..... 63

Chapter 1. Introduction

This thesis focuses on utilizing deep learning to reversely design the cellulose nanocrystal (CNC) nanocomposite film adhering to the white light-emitting diode (WLED) module for improving its performance. WLED is a common and promising device in outdoor and indoor lighting applications. Considering the differences in end-use circumstances, the structures and materials of WLEDs need to be modified to fulfill a variety of demands and conditions. CNC-based optical diffusers have already been verified to change the performances of WLED. The traditional method to design the CNC nanocomposite film (i.e. film pattern and CNC concentration) is achieved by trial and error, which are complex and time-consuming. Many studies have shown that inverse design problems can be efficiently solved by deep learning. Thus, this thesis will explore how machine learning can be used for inverse design of CNC-based optical diffusers for WLED lighting.

In this chapter, the basic definition of WLED and its figures of merit will be introduced. Furthermore, the neural networks of deep learning approaches used in recent photonic research will be summarized. In the end, the targets and rationale of this thesis will be discussed.

1.1 Introduction to white light-emitting diode (WLED)

1.1.1 What is a WLED

A conventional light-emitting diode (LED) is a semiconductor device that can emit light, mostly in the visible region of the electromagnetic spectrum, when applied current flows through it.¹ The emitted light has a relatively narrow spectrum, about 20-30 nm of the full width at half maximum (FWHM) for most LEDs. However, a WLED is preferred for indoor and outdoor lighting (or called illumination) for its wide spectrum covering most of the spectrum in the visible region.² Prior to the vast deployment of WLEDs for illumination, white-light sources are incandescent light bulbs

and compact fluorescent lamps. But these devices are not efficient in energy utilization compared to WLEDs.³ Thus, for most indoor and street lighting applications, WLEDs are replacing previous white-light devices due to their superior properties of high energy efficiency, long lifetime, and low cost.⁴

In order to realize white light, three LED chips that radiate light of three primary colors (red, green, and blue) can be integrated together and colors are mixed to produce white light.³ Some studies also show that the combination of purple LED chips and yellow-green phosphors can efficiently emit white light.⁵ However, as shown in Fig. 1-1 (a), the most common and economical approach to achieve white illumination is to use yellow phosphor-converted WLED,³ which involves a blue LED chip embedded in a thin layer of yellow YAG ($Y_3Al_5O_{12}:Ce^{3+}$) phosphors. In this device, phosphors absorb the blue light produced by a LED chip and generate yellow light. The remaining blue light is combined with the yellow light to create a white spectrum and appears white to human eyes, as shown in Fig. 1-1 (b).

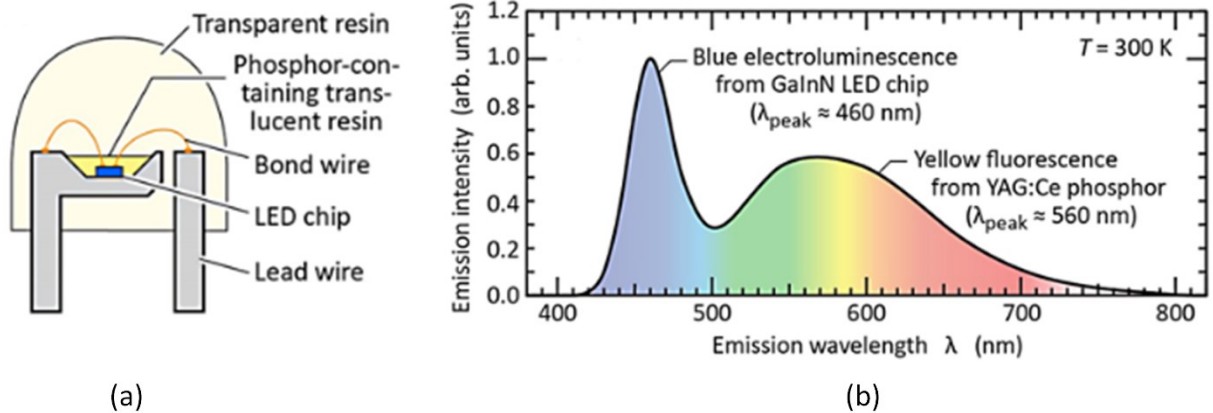


Figure 1-1: (a) The typical structure of WLED. (b) Emission spectrum of the white LED. **Reprinted with permission from Copyright © 2017 by WILEY-VCH Verlag GmbH & Co. KGaA, Weinheim.**³

1.1.2 Figures of merit of WLEDs

The performance of WLED are mainly evaluated using two figures of merit: luminous flux and angular color uniformity (ACU). Here, we will discuss the definition and importance of these two critical performance metrics.

Luminous flux

The measure of the total power of electromagnetic radiation, including infrared, ultraviolet, and visible light, is called radiant flux.⁶ The SI unit of radiant flux is the watt (W) or joule per second (J/s). Assuming that the radiated energy is set as Q joule, the radiant flux can be defined as $\Phi_e = \frac{dQ}{dt}$. Although it has considered the total power radiated from the light source, the radiant flux for each wavelength is different. Hence for the entire optical range of wavelength, the radiant flux function can be written as⁷

$$\Phi_e = \int_0^{\infty} \Phi_e(\lambda) d\lambda.$$

One example of the measured radiant spectrum of radiant flux for WLED is shown in Fig. 1-2.⁸

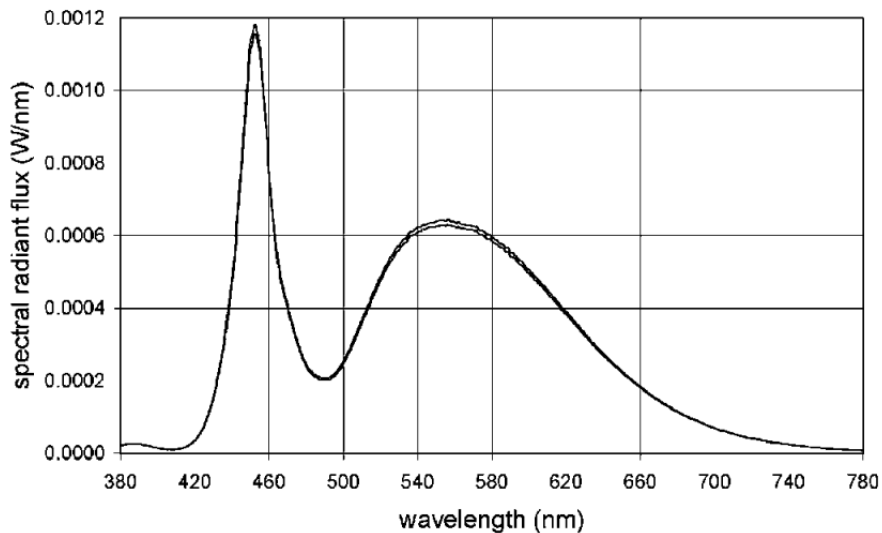


Figure 1-2: An example of the spectral radiant flux of a WLED. **Reprinted by permission from IOP Publishing Ltd: Measurement Science and Technology, copyright (2009).**⁸

Unlike radiant flux, luminous flux only measures the total amount of visible light emitted by a light source, which considers the various sensitivity of human eyes according to different wavelengths of light.⁷ The SI unit for luminous flux is the lumen (lm). The term for brightness measurement based on a normalized model of the sensitivity of the human eye is luminous efficiency. The rod and cone cells in the retinas of the human eye perform two different functions in vision. Under moderate and high levels of illumination, the vision is called photopic vision. In contrast, vision at a low level of intensity of light is named scotopic vision. The two curves in Fig. 1-3 represent the sensitivity of eyes to all wavelengths, the standard light efficiency functions ($V(\lambda)$) for both photopic and scotopic vision, respectively.⁶

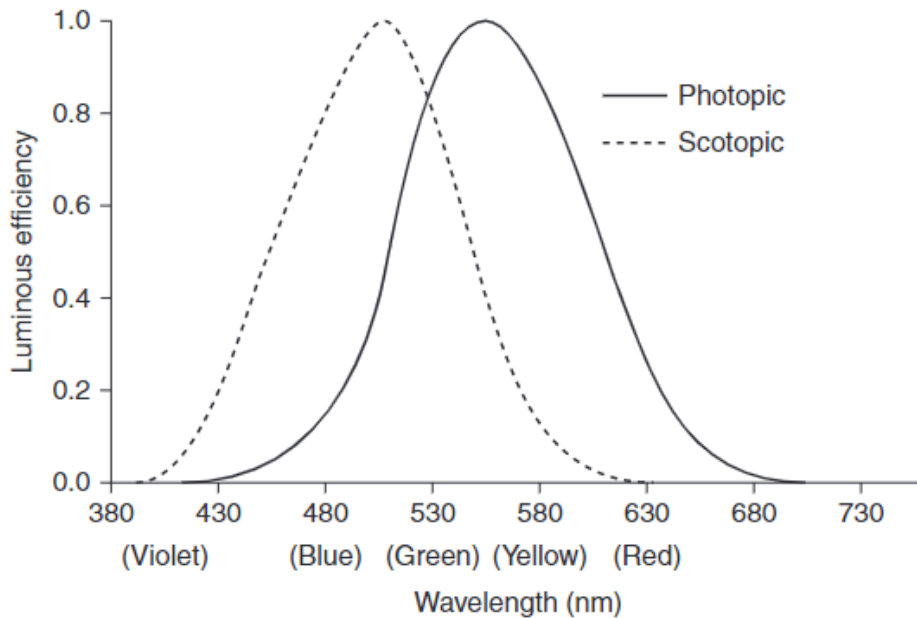


Figure 1-3: Standard luminous efficiency functions. **Reprinted by permission from Copyright © 2014 Woodhead Publishing Limited.**⁶

In order to calculate the luminous flux for one specific wavelength of light, the radiant flux will be multiplying with the corresponding standard luminous efficiency (V_λ) based on Fig. 1-3 and then the result needs to be further multiplied with the maximum spectral luminous efficiency (K_m) which is a constant of 683 lm/W. The equation can be written as ⁶

$$\Phi_V = K_m * \Phi_e * V_\lambda.$$

Therefore, the ability of visible illumination for WLED is determined by luminous flux. For WLED that has a distributed spectrum, the first step is to calculate the integral of the radiant power for each wavelength multiplied by standard luminous efficiency obtained from eye sensitivity map from 380 to 780 nm, and then similarly multiplied by the maximum spectral luminous efficiency to output the overall luminous flux, as shown in the following formula:

$$\Phi_V = K_m \int_{380 \text{ nm}}^{780 \text{ nm}} \Phi_e V_\lambda d\lambda$$

Angular color uniformity (ACU)

As another important figure of merit, ACU reflects the uniformity of correlated color temperature (CCT) from the WLED module. The color temperature of light can be obtained by comparing it to the hue of light that an ideal black-body radiator radiates.⁶ The unit of color temperature is absolute temperature, the kelvin(K). As one characteristic of visible light, color temperature plays a significant role in lighting, manufacturing, photography, and other areas.

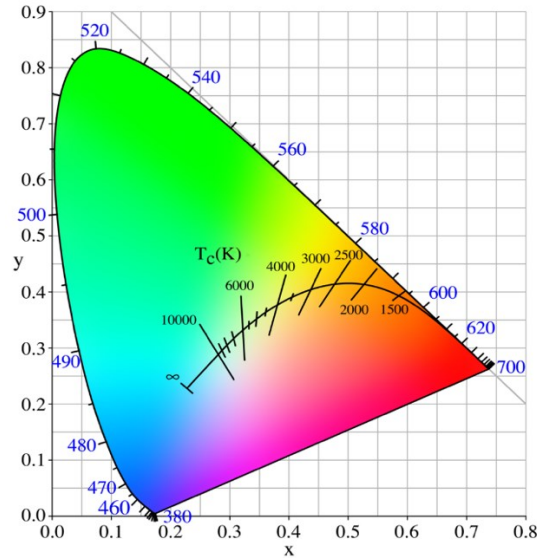


Figure 1-4: The CIE 1931 chromaticity coordinates. **Reprinted by permission from Copyright © 2020 Elsevier Ltd.**⁶

The set of color temperatures is located on the Planckian locus, which is the locus that plots the chromaticity coordinates of the black body radiators that produce light as the change of thermal energy. In order to match the spectrum of a black body to the light source that is non-Planck, the concept of correlated color temperature (CCT) is defined to fulfill a wide range of colors. The CCT of the light source is explained by locating the temperature of the black body radiator, whose color is most closely to that of the light source. Fig. 1-4 shows the chromaticity coordinates that present the hues of black-body light sources of various temperatures and the lines of CCT.⁹ Currently, the illumination industry default identifies the CCT between 2700 K and 3500 K as warm white light, and the cool light source ranging from 4500 K to 7500 K. For the light space illuminated from WLED, the high and low color temperature at different angles create the blueish type of cool white light and yellowish type of warm light, respectively. The unequal distribution of CCT brings about non-uniform and uneven emissions of white light from the WLED module, which causes an undesirable phenomenon named “yellow ring”. Therefore, high ACU is the essential demand for enhancing the performance of WLED.

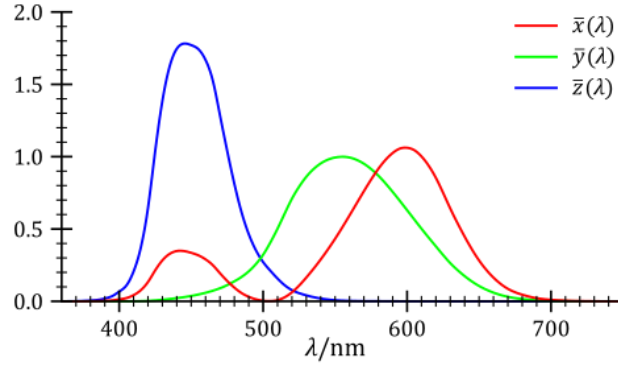


Figure 1-5: The CIE XYZ standard observer color matching functions. **Reprinted by permission from Copyright © 2010 Woodhead Publishing Limited.**⁶

The previous study has built a cubic approximation¹⁰ to calculate the CCT based on the tristimulus values and chromaticity coordinates. The tristimulus value is an expression of the amount of the three primary colors that cause the human retina to perceive a certain color, and the three results are expressed as X, Y, Z. To calculate the tristimulus values, the CIE's color matching functions ($\bar{x}(\lambda)$, $\bar{y}(\lambda)$ and $\bar{z}(\lambda)$) are used to numerically describe the chromatic response of the observer, as shown in Fig. 1-5.¹¹ Combined with the emission intensity ($E(\lambda)$) that can be obtained from the WLED spectrum, the three functions can be expressed as

$$trtmsX = \int_{380}^{780} \bar{x}(\lambda)E(\lambda) d\lambda, \quad trtmsY = \int_{380}^{780} \bar{y}(\lambda)E(\lambda) d\lambda, \quad trtmsZ = \int_{380}^{780} \bar{z}(\lambda)E(\lambda) d\lambda.$$

After acquiring the tristimulus values, the next calculation is to convert the X and Y values to chromaticity values, and the converting function is shown in the following equations:

$$chmtx = \frac{trtmsX}{trtmsX + trtmsY + trtmsZ}, \quad chmty = \frac{trtmsY}{trtmsX + trtmsY + trtmsZ}.$$

The final calculation of CCT is to implement the chromaticity values into the cubic approximation, as shown in the following equation:

$$CCT = 437 * n^3 + 3601 * n^2 + 6861 * n + 5571, \text{ where } n = (chmtx - 0.3320)/(0.1858 - chmty).$$

1.1.3 Conventional methods to improve the performance of WLEDs

By modifying the inner WLED structure, methods have been proposed to improve the luminous flux for WLED, such as changing a sapphire substrate in a cone-shaped nanopattern.¹² By patterning substrate, this structure can improve the crystalline quality of GaN-based LEDs and improve the light output of WLED. The dual structure phosphor layer has also been verified to enhance the luminous efficiency of WLED, as shown in Fig. 1-6.¹³ By inserting a thin silicone layer into the phosphor layer, the light output can be improved because the new added layer optimizes the ratio of the different layers with the increased transmission. The luminous flux can also be improved by applying GaN nanoparticles and GODs as phosphor and charge-transfer medium, respectively.¹⁴ In this method, GODs-based phosphors provide better thermal stability by using this composite film due to the excellent thermal conductivity of GODs, which results in high luminous efficacy and color quality.

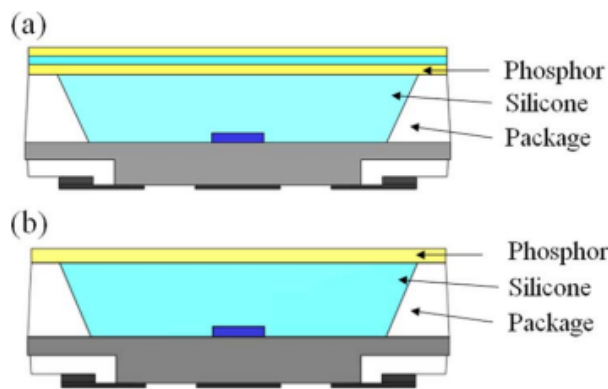


Figure 1-6: Schematic cross-sectional view of (a) dual-layer and (b) conventional remote phosphor structures.

Reprinted with permission from Copyright © 2020 The Institution of Engineering and Technology.³

In order to produce good ACU, conformal phosphor structure has been employed, since it can reduce the CCT deviation. However, it may cause considerable light reflection, which leads to poor

light extraction.¹⁵ The color homogeneity of the WLEDs can be improved by utilizing different remote phosphor packaging methods and reconstructing the factors such as surface curvature and locations of the phosphors.¹⁶ Other methods have also been addressed to enhance the homogeneity of the WLED by carefully designing the silicon lens, or even applying the freeform lens design.^{17,18} Meanwhile, previous research indicates that combining TiO₂ nanoparticles into the materials used in the packaging can resemble a graded-refractive-index multilayer structure.¹⁹ Some works also show the uniformity of CCT can be realized by changing the dispersibility and surface of TiO₂ nanoparticles.²⁰ Another method uses blue laser irradiation to maintain the spatial distribution of the spatial phosphor to improve angular color uniformity.²¹ By considerably influencing the optical path to modify the deviation of CCT, as the use of different MgO nanoparticle concentrations with red phosphor thin films (PTFs) can improve the uniformity of CCT,²² as shown in Fig. 1-7. A recent report presents that boron nitride nanoparticles can be used in an inverted packaging structure to enhance its reflection.²³

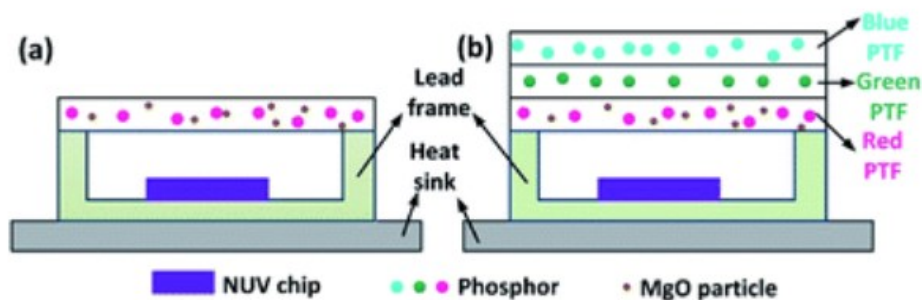


Figure 1-7: Schematic diagram of PTFs: (a) red LED, (b) laminated white LED. *Reprinted with permission from Copyright © The Royal Society of Chemistry 2019.*³

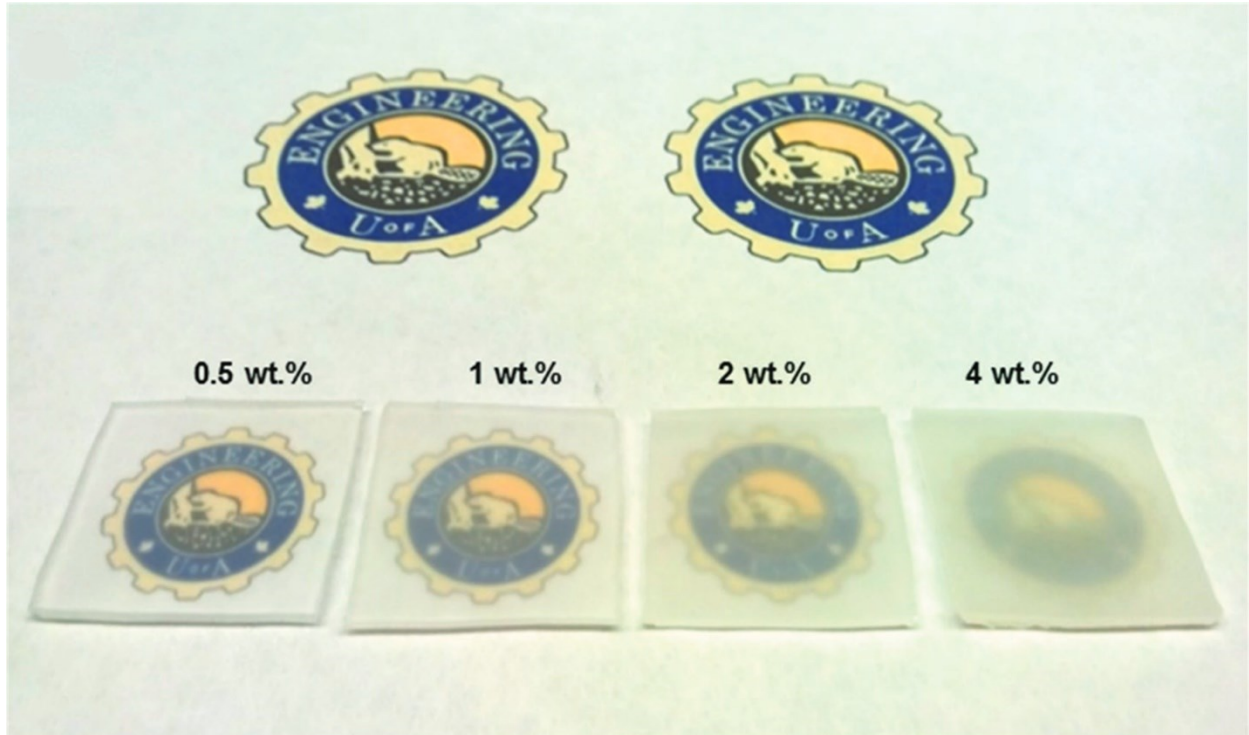
1.2 Improving the performance of WLEDs by employing cellulose-nanocrystal (CNC)-based optical diffusers

In optics, optical diffusers are used to produce soft light by scattering light with evenly spatial and directional intensity distribution. Due to the outstanding light scattering properties of optical diffusers, they have been used in a wide variety of industrial applications for brightness improvement, uniform backlighting, and efficiency enhancement in light-emitting diodes,²⁴⁻²⁶ solar cells,²⁷⁻²⁹ photodetectors,³⁰⁻³² and liquid crystal displays (LCDs).³³⁻³⁵ Optical diffusers are often manufactured based on translucent materials such as different types of glass. Previously, our group proposed that CNC-filled polymer is an effective optical diffuser material and improves ACU by coating a thin film layer on a WLED module.

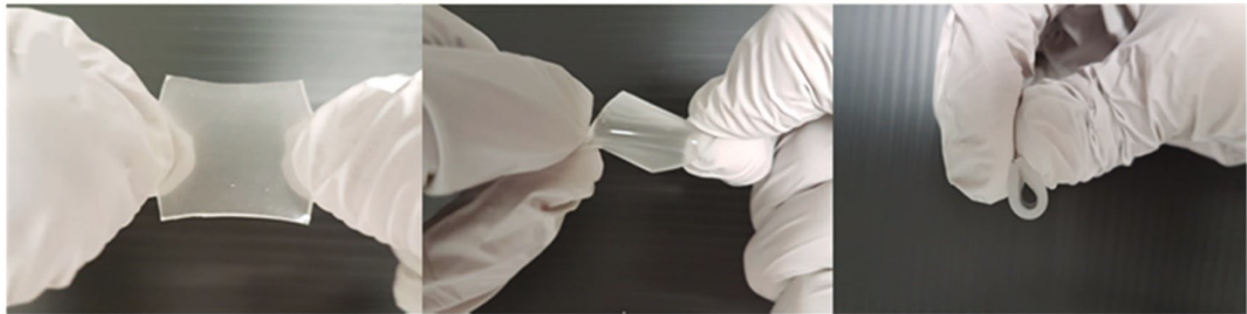
1.2.1 Superior properties of CNC as an optical diffuser on WLED modules

CNC, an environmentally friendly material, is non-toxic and biodegradable and can be extracted from natural sources such as woody biomass or other fiber supplies available in plants.³⁶ Because CNC is a high-molecular-weight linear polymer generated from monomers linked together by glycosidic oxygen bridges, they provide superior bulk and nanoscale properties such as high tensile strength, low density, and large surface area. With these excellent advantages, CNC has been used as a substrate in devices of sensors,³⁷ solar cells,³⁸ transistors,³⁹ and LEDs.⁴⁰ Meanwhile, due to the rod-like shape and wavelength scale on the order of hundreds of nanometers, CNC-filled polymer can provide magnificent broadband light softening in the visible and near-visible regions of light. Our group's previous study has doped CNC into polydimethylsiloxane (PDMS), and the CNC nanocomposite film can be used as an excellent optical diffuser to improve the ACU of WLED. Fig. 1-8 (a) shows that variation in the transparency and light diffusion behavior can be observed while the CNC concentration increases. The concentration of CNC doped in the polymer is represented by weight percentage. A high concentration of CNC filled in PDMS causes high light scattering properties and less transparency, which agrees with the changes of transparency and haze with a high density of filling material for other volumetric types of optical diffusers.

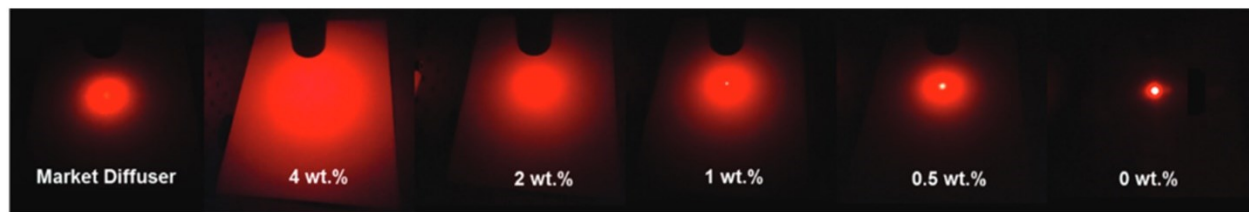
Furthermore, Fig. 1-8 (b) also shows the flexibility and mechanical properties of CNC nanocomposite film as optical diffusers to resist extreme physical pressure, such as stretching, twisting, and bending, without losing their other properties. In terms of the scattering mechanism, clusters of aggregated CNCs in the matrix materials lead to significant insensitivity to accepting the incident light. Less dependent on the wavelength of light compared to Rayleigh scattering, Mie scattering can be considered the dominant scattering method of CNC nanocomposite film. In the CNC nanocomposite model, the CNC particle size is 3 μm . The CNC and polymer matrix refractive indices are 1.6 and 1.4, respectively. As shown in Fig. 1-8 (c), a 635 nm laser beam is scattered by the CNC nanocomposite film with different concentrations and compared to the market diffuser. The results show that 1 wt.% of CNC filled-in polymer can realize similar light diffusion ability as the performance of the market diffuser.



(a)



(b)



(c)

Figure 1-8: (a) Picture of CNC nanocomposite film-based optical diffuser with different CNC concentrations (0.5, 1, 2, 4 wt.%) (b) The physical properties of the diffusers withstand the applications of twisting, stretching, and

*bending. (c) Optical diffusion of a 635 nm laser beam by CNC nanocomposite film-based optical diffusers with different concentrations (wt%) of CNC and compared with market diffusers. Reprinted with permission from Copyright © 2017 by WILEY-VCH Verlag GmbH & Co. KGaA, Weinheim.*³

Furthermore, based on the incident light from the same laser beam, Fig. 1-9, illustrates the ACU after passing different concentrations of CNC nanocomposite film. With the increase of concentration of filler material, the light scattering angle becomes more expansive and the ACU is more uniform and inconsistent with the observed changes. For the sample with a CNC concentration of 4 wt%, the intensity distribution is very close to an ideal diffuse reflective surface with a Lambertian distribution (dashed line). It underscores the light-diffusing ability of the optical diffuser based on CNC-filled polymer has the ability to provide a Lambertian-like distribution of fill material at a concentration of only 4 wt% of filling material.

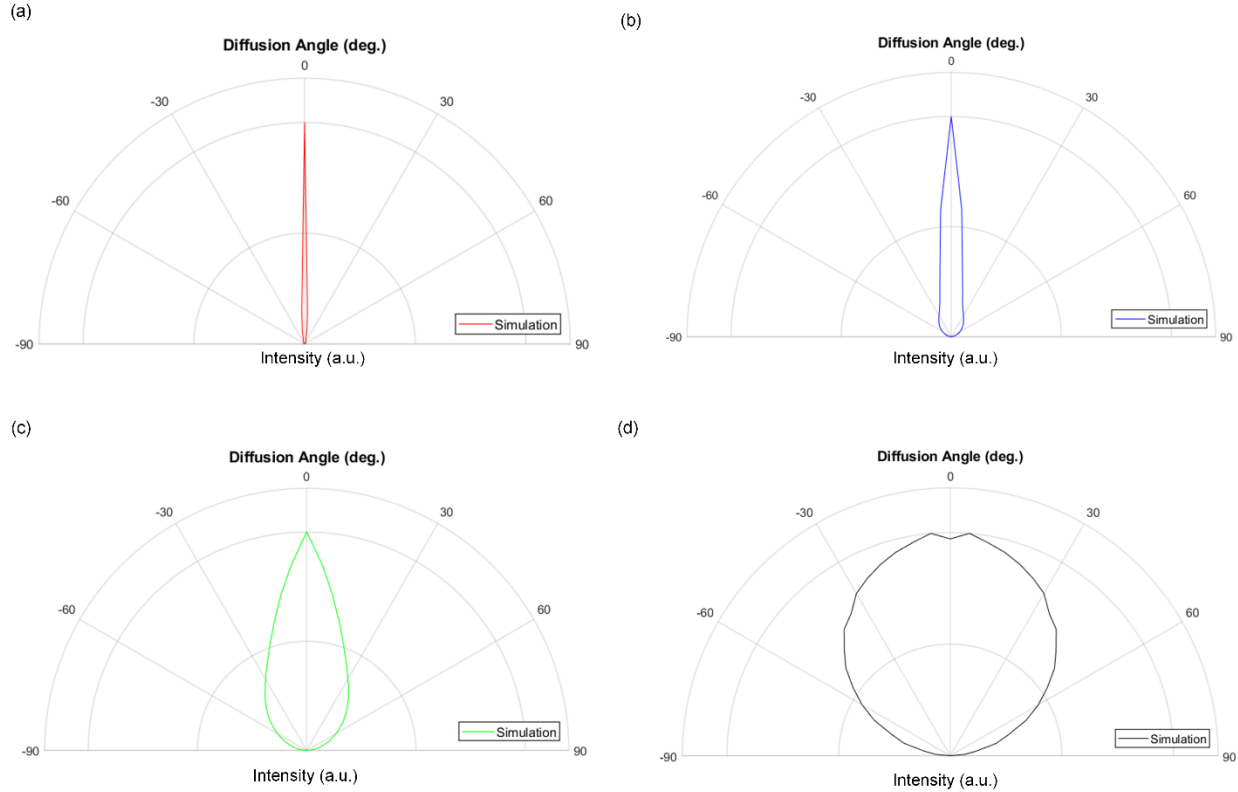


Figure 1-9: ACU of a 635 nm laser beam after passing through CNC nanocomposite film-based optical diffuser with different concentrations of CNC: (a) 0.5, (b) 1, (c) 2, and (d) 4 wt%.

1.2.2 Challenges in design related parameters of CNC film pattern

The industrial application generally needs to obtain a WLED product that can reach specific sets of performances. As discussed above, CNC filled-polymer-based optical diffuser effectively improves ACU with its light scattering ability. In order to achieve a well-defined numerical combination of these two properties, the standard approach first requires designing the shape of the CNC nanocomposite film. However, our previous research indicates that a simple central coverage shape with one coverage angle must be designed to improve ACU but decrease the luminous flux. Therefore, in order to balance the two performances, more complex shapes with plenty of structural parameters of CNC nanocomposite film need to be designed. Furthermore, the film thickness and concentration of the CNC in the nanocomposite film can effectively affect

the light diffusion ability due to an increase in the total quantity of CNC nanocomposite film used. The workflow of a traditional and complete design method for certain performance sets is trial-and-error learning, which needs to iteratively run simulations and experiments based on lots of sets of structural parameters, thickness, and concentrations. It is tedious and highly time-consuming and requires experienced optical designers for practical application.

1.3 Applying deep learning to the inverse design of optical diffusers for WLED modules

Over the past two decades, machine learning has been applied to address questions in many scientific studies and engineering applications. In machine learning, specific tasks are assigned to a computer program, and the machine is said to have learned the experience, while the visual performance in those tasks enhances with more and more experience performing those tasks. Machine learning is a data-driven technique that can make decisions and predictions based on the existing data or the learning experience. Deep learning as a new branch of machine learning has attracted much attention, and new models proposed in deep learning produce better performance in analyzing questions in various areas. Here we make a brief survey of the deep learning models used for inverse design in the photonic research.

1.3.1 What is deep learning?

Deep learning allows computational models composed of multiple hidden layers to learn data representations with multiple levels of abstraction.⁴¹ Besides, representation learning is a method that allows machines to automatically search and find the features and representations based on raw data. As one of the representation learning techniques, deep learning can achieve multiple levels of representations through the nonlinear combination of plenty of modules.⁴² Each one can transfer a low-level representation to a representation at the high level, which generally has more abstract features. With this complicated and nonlinear multilayer structure, deep learning can

learn complex functions and effectively employ model fitting to realize feature learning.⁴³ Currently, deep learning has emerged in many areas, broadly from laboratory research to industries, while concerned about data-intensive issues, such as speech recognition, computer vision, and natural language processing. Furthermore, for other applications, research has already recognized that it can be more convenient to train a system by collecting and inserting examples of demand input-output behaviour than manually trying all possible samples and anticipating the desired response by experiments or simulations.⁴⁴ Meanwhile, deep learning has been used in photonics and optical area as one powerful computational method to solve problems such as inverse design.

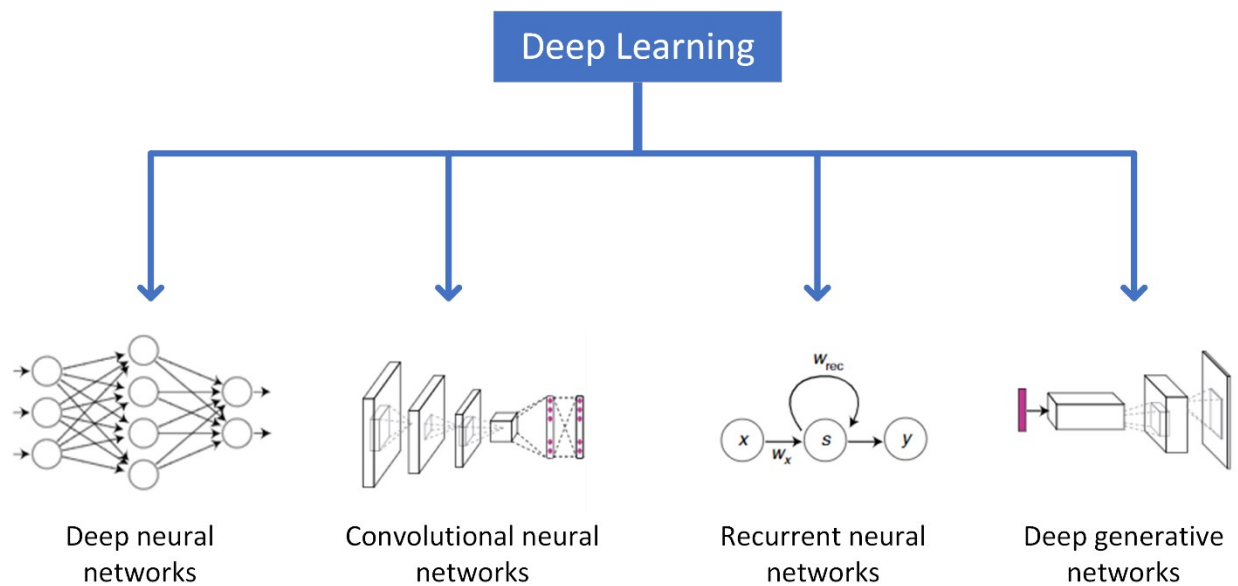


Figure 1-10: The schematics of the main neural network architectures in deep learning.

1.3.2 Different types of neural networks involved in the photonic research

Advanced deep learning model architectures have been proposed to solve tasks and can be generally divided into four categories which are deep neural network (DNN), convolutional neural network (CNN), recurrent neural network and deep generative models, as shown in Fig. 1-10.

DNN as the foundation of modern neural networks has the superior ability to extract high-level features from raw data. DNN has multilayered architectures, and each hidden layer is constructed with sufficient neuron units which support this model to learn complex input-output relationships based on the approximation theorem. Previous reports show that a bidirectional DNN-based architecture can be trained to inverse design the plasmonic nanostructure.⁴³ They transfer the H-shaped metallic structure to eight parameters, including the three continuous parameters (the rotation and length of arms) and five binary parameters representing the existence of certain arms. The desired performances are set as material properties, vertical and horizontal spectrum and each of them has 43 neurons in the output layer. Similarly, another study proposes a deep neural network with two bidirectional neural networks that can achieve the on-demand chiral metamaterials design and collect corresponding responses when receiving specific incident light.⁴⁵ Applying the convolution operations, convolution neural networks have been used to extract features from the high-dimensional raw data. Recent research works have realized the photonics problem that inputs are plenty of images, such as inverse scattering of nonlinear electromagnetic waves.⁴⁶⁻⁴⁹ Additionally, recurrent neural networks are a type of artificial neural network in that connections between each node can create a loop, allowing the output of some nodes to affect subsequent inputs of the same node, which leads to the behavior of temporal dynamics. The previous study applied recurrent neural networks capable of learning sequential data to analyze optical signals and noise in high-speed fiber optic transmission.⁵⁰⁻⁵² To accomplish the generating of new data similar to the original training samples, deep generative networks can provide innovative and unseen results. Generative adversarial network (GAN) and variational autoencoder (VAE) as practical applications of deep generative models have realized image generation in recent years. Especially, GAN is the famous model of the deep generative network because it has two neural networks inside, named generator and discriminator, which compete with each other to realize better accuracy and performance in their anticipation. In

photonics, GAN has been commonly used to achieve the efficient inverse design of hypersurfaces with training images as input.⁵³⁻⁵⁵

1.4 Objectives and outline of the thesis

Improving the performance of WLED is of interest to academia and industry in illumination application. Most developments reported in journals focus on modifying the materials or structures inside WLED. Besides, some emerging materials with excellent optical properties have also been developed to be used as optical diffusers adhering to the WLED module. However, these optical diffusers are built to cover whole or most of surface of the WLED module, therefore, luminous flux and ACU cannot be optimized at the same time. In this thesis, we show that deep learning is a superior data analysis method that can be used to solve the abovementioned challenges. Based on the well-trained neural network models, any intuitive inverse design of optical diffusers can be replaced by machine learning, and the new deep learning approach can produce even better results. Furthermore, optical diffusers have never been shown to control brightness distribution of WLEDs, since only lenses and mirrors are considered as optical devices to focus light and generate brightness patterns. After successfully building and training the neural network to solve the problem in this first project, we extended the application to three-dimensional geometry, and we set up the objective to obtain the desired brightness distribution using optical diffusers. This work paves the way to apply scattering optics for WLED lighting, beyond the use of lenses and mirrors.

In chapter 1, we show the basic definition of WLEDs and the description of CNC nanocomposite film-based optical diffusers. Additionally, we will provide a brief review of the recent development of inverse design of photonic structures by deep learning.

In chapter 2, we demonstrate a deep learning-based inverse design method to design CNC nanocomposite films coated on WLED modules. To collect data sets, we varied different

parameter sets involving angles of the shapes, thickness, and concentration of the CNC films. After that, we trained forward neural networks based on the original data sets and used a pretrained forward model to build the total inverse design architecture. We implemented deep learning to predict the parameter sets according to the desired performances. We further utilized the pretrained forward neural network to search for CNC nanocomposite films with the best performance.

In chapter 3, we tackle a new problem using the coated CNC composite films and apply the spherical convolutional neural network (CNN) in deep learning to inversely design the concentration distributions inside the CNC nanocomposite film for desired brightness distribution from WLEDs. In this study, we focused on the pattern of the CNC nanocomposite film in three-dimensional. We first broke the whole CNC film into 168 triangles and set up the output to be the brightness distribution in hemisphere spatial space. By training spherical CNN architecture, we found new solutions of concentration distributions of CNC in the nanocomposite film which could produce similar brightness distribution, compared to the intuitive design. Besides, to design a gradually changed brightness distribution using nanocomposite films, an intuitive design approach requires plenty of trial-and-error works to search the suitable parameters. While the deep learning method could directly provide the parameter of the CNC nanocomposite film to realize gradually varied brightness distribution.

In chapter 4, we summarize our works and clearly show our contributions to the research field. Then we briefly discuss the future improvement and applications of our inverse design of CNC-based optical diffusers for improving the performance of WLEDs.

Reference:

- (1) Dupuis, R. D.; Krames, M. R. History, Development, and Applications of High-Brightness Visible Light-Emitting Diodes. *Journal of Lightwave Technology*. May 1, **2008**, pp 1154–1171. <https://doi.org/10.1109/JLT.2008.923628>.
- (2) Nair, G. B.; Dhoble, S. J. A Perspective Perception on the Applications of Light-Emitting Diodes. *Luminescence*. John Wiley and Sons Ltd December 1, **2015**, pp 1167–1175. <https://doi.org/10.1002/bio.2919>.
- (3) Cho, J.; Park, J. H.; Kim, J. K.; Schubert, E. F. White Light-Emitting Diodes: History, Progress, and Future. *Laser and Photonics Reviews*. Wiley-VCH Verlag March 1, **2017**. <https://doi.org/10.1002/lpor.201600147>.
- (4) Pust, P.; Schmidt, P. J.; Schnick, W. A Revolution in Lighting. *Nature Materials*. Nature Publishing Group May 1, **2015**, pp 454–458. <https://doi.org/10.1038/nmat4270>.
- (5) Shibata, N.; Uemura, T.; Yamaguchi, H.; Yasukawa, T. Fabrication of LED Based on III-V Nitride and Its Applications. *Physica Status Solidi A Appl Res* **2003**, *200* (1), 58–61. <https://doi.org/10.1002/pssa.200303540>.
- (6) Choudhury, A. K. R. Characteristics of Light Sources. In *Principles of Colour and Appearance Measurement*; Elsevier, **2014**; pp 1–52. <https://doi.org/10.1533/9780857099242.1>.
- (7) R. John Koschel, "Introduction and Terminology," in *Illumination Engineering: Design with Nonimaging Optics*, *IEEE*, **2013**, pp.1-30, <https://doi.org/10.1002/9781118462539.ch1>.
- (8) Hanselaer, P.; Keppens, A.; Forment, S.; Ryckaert, W. R.; Deconinck, G. A New Integrating Sphere Design for Spectral Radiant Flux Determination of Light-Emitting Diodes. *Meas Sci Technol* **2009**, *20* (9). <https://doi.org/10.1088/0957-0233/20/9/095111>.
- (9) Bertalmío, M. Colour Representation and Colour Gamuts. *Vision Models for High Dynamic Range and Wide Colour Gamut Imaging* **2020**, 131–155. <https://doi.org/10.1016/B978-0-12-813894-6.00011-9>.
- (10) McCamy, C. S. Correlated Color Temperature as an Explicit Function of Chromaticity Coordinates. *Color Res Appl* **1992**, *17* (2), 142–144. <https://doi.org/10.1002/col.5080170211>.
- (11) Macdougall, D. B. Colour Measurement of Food: Principles and Practice. *Colour Measurement: Principles, Advances and Industrial Applications* **2010**, 312–342. <https://doi.org/10.1533/9780857090195.2.312>.
- (12) Huang, J. K.; Lin, D. W.; Shih, M. H.; Lee, K. Y.; Chen, J. R.; Huang, H. W.; Kuo, S. Y.; Lin, C. H.; Lee, P. T.; Chi, G. C.; Kuo, H. C. Investigation and Comparison of the Gan-Based Light-Emitting Diodes Grown on High Aspect Ratio Nano-Cone and General Micro-Cone Patterned Sapphire Substrate. *IEEE/OSA Journal of Display Technology* **2013**, *9* (12), 947–952. <https://doi.org/10.1109/JDT.2013.2270276>.

- (13) Chen, K. J.; Chen, H. C.; Shih, M. H.; Wang, C. H.; Tsai, H. H.; Chien, S. H.; Lin, C. C.; Kuo, H. C. Enhanced Luminous Efficiency of WLEDs Using a Dual-Layer Structure of the Remote Phosphor Package. *Journal of Lightwave Technology* **2013**, *31* (12), 1941–1945. <https://doi.org/10.1109/JLT.2013.2260322>.
- (14) Kumar, M.; Sunny; Kumar, A.; Seong, K. S.; Park, S. H. GaN Phosphors Converted White Light-Emitting Diodes for High Luminous Efficacy and Improved Thermal Stability. *IET Optoelectronics* **2020**, *14* (4), 155–158. <https://doi.org/10.1049/iet-opt.2019.0084>.
- (15) Liu, Z.; Liu, S.; Wang, K.; Luo, X. *Optical Analysis of Color Distribution in White LEDs with Various Packaging Methods*; **2002**; Vol. 194.
- (16) Liu, Z.; Liu, S.; Wang, K.; Luo, X. Optical Analysis of Color Distribution in White LEDs with Various Packaging Methods. *IEEE Photonics Technology Letters* **2008**, *20* (24), 2027–2029. <https://doi.org/10.1109/LPT.2008.2005998>.
- (17) Chen, J.-J.; Wang, T.-Y.; Huang, K.-L.; Liu, T.-S.; Tsai, M.-D.; Lin, C.-T.; Ries, H.; Muschaweck, J.; Benítez, P.; Miñano, J. C.; Blen, J.; Mohedano, R.; Chaves, J.; Dross, O.; Hernández, M.; Falicoff, W.; Liu, Q.; Gao, H.; Yu, F.; Li, L.; Wang, D.; Zhang, Y. *Fast Freeform Reflector Generation Using Source-Target Maps*; W, **2002**; Vol. 19.
- (18) Yu, S.; Li, Z.; Liang, G.; Tang, Y.; Yu, B.; Chen, K. Angular Color Uniformity Enhancement of White Light-Emitting Diodes by Remote Micro-Patterned Phosphor Film. *Photonics Res* **2016**, *4* (4), 140. <https://doi.org/10.1364/prj.4.000140>.
- (19) Mont, F. W.; Kim, J. K.; Schubert, M. F.; Schubert, E. F.; Siegel, R. W. High-Refractive-Index TiO₂ Nanoparticle-Loaded Encapsulants for Light-Emitting Diodes. *J Appl Phys* **2008**, *103* (8). <https://doi.org/10.1063/1.2903484>.
- (20) Song, G. Y.; Jang, I.; Jeon, S. W.; Ahn, S. H.; Kim, J. Y.; Sa, G. Controlling the Surface Properties of TiO₂ for Improvement of the Photo-Performance and Color Uniformity of the Light-Emitting Diode Devices. *Journal of Industrial and Engineering Chemistry* **2021**, *94*, 180–187. <https://doi.org/10.1016/J.JIEC.2020.10.031>.
- (21) Liu, J.; Lu, X.; Wang, W.; Su, Z.; Xing, B.; Zheng, H.; Liu, S. Tailoring Particle Distribution for White LEDs with High Color-Uniformity by Selective Curing. *IEEE Photonics Technology Letters* **2021**, *33* (4), 193–196. <https://doi.org/10.1109/LPT.2020.3046740>.
- (22) Zhuo, N.; Zhang, N.; Chen, P.; Wang, H. Enhancement of Efficiency and CCT Uniformity for Red Phosphor Thin Films, Red LEDs and Laminated White LEDs Based on near-Ultraviolet LEDs Using MgO Nanoparticles. *RSC Adv* **2019**, *9* (48), 28291–28298. <https://doi.org/10.1039/c9ra06069c>.
- (23) Li, Z. T.; Liang, J. Y.; Li, J. S.; Li, J. X.; Tang, Y. Scattering Nanoparticles-Induced Reflection Effect for Enhancing Optical Efficiency of Inverted Quantum Dots-Light-Emitting Diodes Combined with the Centrifugation Technique. *Journal of Electronic Packaging, Transactions of the ASME* **2021**, *143* (2). <https://doi.org/10.1115/1.4048034>.
- (24) Yang, X.; Dev, K.; Wang, J.; Mutlugun, E.; Dang, C.; Zhao, Y.; Liu, S.; Tang, Y.; Tan, S. T.; Sun, X. W.; Demir, H. V. Light Extraction Efficiency Enhancement of Colloidal Quantum Dot Light-Emitting

- Diodes Using Large-Scale Nanopillar Arrays. *Adv Funct Mater* **2014**, *24* (38), 5977–5984.
<https://doi.org/10.1002/adfm.201400190>.
- (25) Zhou, L.; Dong, X.; Zhou, Y.; Su, W.; Chen, X.; Zhu, Y.; Shen, S. Multiscale Micro-Nano Nested Structures: Engineered Surface Morphology for Efficient Light Escaping in Organic Light-Emitting Diodes. *ACS Appl Mater Interfaces* **2015**, *7* (48), 26989–26998.
<https://doi.org/10.1021/acsami.5b08575>.
- (26) Chen, C.-Y.; Chen, Y.-J.; Lee, W.-K.; Lu, C.-Y.; Lin, H. Y.; Wu, C.-C. Analyses of Optical Out-Coupling of Organic Light-Emitting Devices Having Micromesh Indium Tin Oxide and Conducting Polymer as Composite Transparent Electrode. *Opt Express* **2016**, *24* (10), A810.
<https://doi.org/10.1364/oe.24.00a810>.
- (27) Mahpeykar, S. M.; Xiong, Q.; Wang, X. Resonance-Induced Absorption Enhancement in Colloidal Quantum Dot Solar Cells Using Nanostructured Electrodes. *Opt Express* **2014**, *22* (S6), A1576.
<https://doi.org/10.1364/oe.22.0a1576>.
- (28) Chen, C.-Y.; Chen, Y.-J.; Lee, W.-K.; Lu, C.-Y.; Lin, H. Y.; Wu, C.-C. Analyses of Optical Out-Coupling of Organic Light-Emitting Devices Having Micromesh Indium Tin Oxide and Conducting Polymer as Composite Transparent Electrode. *Opt Express* **2016**, *24* (10), A810.
<https://doi.org/10.1364/oe.24.00a810>.
- (29) Zhou, L.; Dong, X.; Zhou, Y.; Su, W.; Chen, X.; Zhu, Y.; Shen, S. Multiscale Micro-Nano Nested Structures: Engineered Surface Morphology for Efficient Light Escaping in Organic Light-Emitting Diodes. *ACS Appl Mater Interfaces* **2015**, *7* (48), 26989–26998.
<https://doi.org/10.1021/acsami.5b08575>.
- (30) Duan, X.; Huang, Y.; Ren, X.; Shang, Y.; Fan, X.; Hu, F. High-Efficiency InGaAs/InP Photodetector Incorporating SOI-Based Concentric Circular Subwavelength Gratings. *IEEE Photonics Technology Letters* **2012**, *24* (10), 863–865. <https://doi.org/10.1109/LPT.2012.2189559>.
- (31) Zhang, X.; Huang, Y.; Ren, X.; Huang, H.; Wang, Q. *Flat-Top Steep-Edge Photodetector with Cascaded Grating Structure*; **2009**.
- (32) Brongersma, M. L.; Cui, Y.; Fan, S. Light Management for Photovoltaics Using High-Index Nanostructures. *Nature Materials*. Nature Publishing Group **2014**, pp 451–460.
<https://doi.org/10.1038/nmat3921>.
- (33) Kuo, H. P.; Chuang, M. Y.; Lin, C. C. Design Correlations for the Optical Performance of the Particle-Diffusing Bottom Diffusers in the LCD Backlight Unit. *Powder Technol* **2009**, *192* (1), 116–121. <https://doi.org/10.1016/j.powtec.2008.12.003>.
- (34) Kim, G. H.; Kim, W. J.; Kim, S. M.; Son, J. G. Analysis of Thermo-Physical and Optical Properties of a Diffuser Using PET/PC/PBT Copolymer in LCD Backlight Units. *Displays* **2005**, *26* (1), 37–43.
<https://doi.org/10.1016/j.displa.2004.11.001>.
- (35) Liu, M.; Wu, D.; Zhang, Y.; Zhuang, J. Optimization and Design of LCD Diffuser Plate with Micro-Semisphere Structure. *Procedia Eng* **2011**, *16*, 306–311.
<https://doi.org/10.1016/J.PROENG.2011.08.1088>.

- (36) Mahpeykar, S. M.; Zhao, Y.; Li, X.; Yang, Z.; Xu, Q.; Lu, Z. H.; Sargent, E. H.; Wang, X. Cellulose Nanocrystal:Polymer Hybrid Optical Diffusers for Index-Matching-Free Light Management in Optoelectronic Devices. *Adv Opt Mater* **2017**, *5* (21). <https://doi.org/10.1002/adom.201700430>.
- (37) Meng, L.; Mahpeykar, S. M.; Xiong, Q.; Ahvazi, B.; Wang, X. Strain Sensors on Water-Soluble Cellulose Nanofibril Paper by Polydimethylsiloxane (PDMS) Stencil Lithography. *RSC Adv* **2016**, *6* (88), 85427–85433. <https://doi.org/10.1039/c6ra10069d>.
- (38) Nogi, M.; Karakawa, M.; Komoda, N.; Yagyu, H.; Nge, T. T. Transparent Conductive Nanofiber Paper for Foldable Solar Cells. *Sci Rep* **2015**, *5*. <https://doi.org/10.1038/srep17254>.
- (39) Wang, C. Y.; Fuentes-Hernandez, C.; Liu, J. C.; Dindar, A.; Choi, S.; Youngblood, J. P.; Moon, R. J.; Kippelen, B. Stable Low-Voltage Operation Top-Gate Organic Field-Effect Transistors on Cellulose Nanocrystal Substrates. *ACS Appl Mater Interfaces* **2015**, *7* (8), 4804–4808. <https://doi.org/10.1021/am508723a>.
- (40) Najafabadi, E.; Zhou, Y. H.; Knauer, K. A.; Fuentes-Hernandez, C.; Kippelen, B. Efficient Organic Light-Emitting Diodes Fabricated on Cellulose Nanocrystal Substrates. *Appl Phys Lett* **2014**, *105* (6). <https://doi.org/10.1063/1.4891046>.
- (41) Lecun, Y.; Bengio, Y.; Hinton, G. Deep Learning. *Nature*. Nature Publishing Group May 27, **2015**, pp 436–444. <https://doi.org/10.1038/nature14539>.
- (42) Horvitz, E.; Mulligan, D. Data, Privacy, and the Greater Good. *Science (1979)* **2015**, *349* (6245), 253–255. <https://doi.org/10.1126/science.aac4520>.
- (43) Malkiel, I.; Mrejen, M.; Nagler, A.; Arieli, U.; Wolf, L.; Suchowski, H. Plasmonic Nanostructure Design and Characterization via Deep Learning. *Light Sci Appl* **2018**, *7* (1). <https://doi.org/10.1038/s41377-018-0060-7>.
- (44) Ma, W.; Liu, Z.; Kudyshev, Z. A.; Boltasseva, A.; Cai, W.; Liu, Y. Deep Learning for the Design of Photonic Structures. *Nature Photonics*. Nature Research February 1, **2021**, pp 77–90. <https://doi.org/10.1038/s41566-020-0685-y>.
- (45) Liao, X.; Gui, L.; Yu, Z.; Zhang, T.; Xu, K. Deep Learning for the Design of 3D Chiral Plasmonic Metasurfaces. *Opt Mater Express* **2022**, *12* (2), 758. <https://doi.org/10.1364/ome.449152>.
- (46) Unni, R.; Yao, K.; Zheng, Y. Deep Convolutional Mixture Density Network for Inverse Design of Layered Photonic Structures. *ACS Photonics* **2020**, *7* (10), 2703–2712. <https://doi.org/10.1021/acsp Photonics.0c00630>.
- (47) Wu, J.; Li, J.; Liu, X.; Gong, L.; Chen, J.; Tang, Z.; Lin, W.; Mu, Y.; Lin, X.; Hong, W.; Yi, G.; Chen, X. Unclonable Photonic Crystal Hydrogels with Controllable Encoding Capacity for Anticounterfeiting. *ACS Appl Mater Interfaces* **2022**, *14* (1), 2369–2380. <https://doi.org/10.1021/acsaami.1c20905>.
- (48) Malkiel, I.; Nagler, A.; Arieli, U.; Mrejen, M.; Wolf, L.; Suchowski, H. *Deep Learning for Design and Retrieval of Nano-Photonic Structures*.

- (49) Li, L.; Wang, L. G.; Teixeira, F. L.; Liu, C.; Nehorai, A.; Cui, T. J. DeepNIS: Deep Neural Network for Nonlinear Electromagnetic Inverse Scattering. *IEEE Trans Antennas Propag* **2019**, *67* (3), 1819–1825. <https://doi.org/10.1109/TAP.2018.2885437>.
- (50) Zhou, Q.; Yang, C.; Liang, A.; Zheng, X.; Chen, Z. Low Computationally Complex Recurrent Neural Network for High Speed Optical Fiber Transmission. *Opt Commun* **2019**, *441*, 121–126. <https://doi.org/10.1016/j.optcom.2019.02.037>.
- (51) Chen, M.; Jiang, J.; Fan, J. A. Algorithm-Driven Paradigms for Freeform Optical Engineering. *ACS Photonics*. American Chemical Society 2022. <https://doi.org/10.1021/acsp Photonics.2c00612>.
- (52) Ferguson, A. L.; Ma, Y.; Alicino, J. C. Inverse Design of Self-Assembling Diamond Photonic Lattices from Anisotropic Colloidal Clusters. *Journal of Physical Chemistry B* **2021**, *125* (9), 2398–2410. <https://doi.org/10.1021/acs.jp cb.0c08723>.
- (53) Wen, F.; Jiang, J.; Fan, J. A. Robust Freeform Metasurface Design Based on Progressively Growing Generative Networks. *ACS Photonics* **2020**, *7* (8), 2098–2104. <https://doi.org/10.1021/acsp Photonics.0c00539>.
- (54) Jiang, J.; Sell, D.; Hoyer, S.; Hickey, J.; Yang, J.; Fan, J. A. Free-Form Diffractive Metagrating Design Based on Generative Adversarial Networks. *ACS Nano* **2019**, *13* (8), 8872–8878. <https://doi.org/10.1021/acsnano.9b02371>.
- (55) Liu, Z.; Zhu, D.; Rodrigues, S. P.; Lee, K. T.; Cai, W. Generative Model for the Inverse Design of Metasurfaces. *Nano Lett* **2018**, *18* (10), 6570–6576. <https://doi.org/10.1021/acs.nanolett.8b03171>.

Chapter 2. Deep learning enabled inverse design of nanocrystal-based optical diffusers for efficient white LED lighting

2.1 Introduction

White light-emitting diodes (WLEDs) have gained popularity in illuminating applications. With superior properties such as high efficiency, long lifespan, and low cost, WLEDs have replaced the traditional incandescent and fluorescent lamps as the new white light source.^{1,2} The most successful and common device to generate white light is the phosphor-converted WLED module.³ A thin layer of yellow YAG ($\text{Y}_3\text{Al}_5\text{O}_{12}:\text{Ce}_3+$) phosphor absorbs blue light created by the LED chip and emits yellow light, which combines with the remaining blue light to form and emit a white spectrum. The two critical figure-of-merits of WLEDs are luminous flux and angular color uniformity (ACU).^{4,5} The main problem encountered with typical designs of WLEDs is the relatively poor ACU. To achieve high ACU for a WLED, previous studies utilized methods such as doping phosphor with TiO_2 nanoparticles and modified conformal phosphor structure.^{6,7} Other approaches involved optimization of WLED substrates and improved lens design to strengthen the uniformity of light.^{8,9} Previously, we have reported an alternative method to enhance ACU by coating a thin film of cellulose-nanocrystal (CNC)-filled polymer on the WLED module as an optical diffuser.¹⁰ CNC as a green material can be mixed with polymer to be fabricated as CNC nanocomposite.¹¹ It can adhere conveniently to the lens surface of the WLED and has been proved to have excellent light scattering ability. Employing nanocrystal-based optical diffusers is a widely used strategy to improve WLED performance. These nanoparticles have been demonstrated for improving ACU (reducing Δ CCT) in WLED lighting in previous reports.^{4-7,10,11} However, improved ACU normally comes with the cost of lowered luminous flux. Therefore, it is of

significance to balance the trade-off that improves ACU while maximizing output luminous flux. Yet, such optimizations like the optimization of lens design in illuminating applications were performed through the trial-and-error learning using simulations or experiments, which are tedious and extremely time-consuming and require experienced optical designers in practical applications.

In recent years, machine learning, as one direction of artificial intelligence, has attracted much attention because it can automatically construct a mathematical model for prediction based on training data sets.¹² Deep learning is a popular branch of machine learning, which employs artificial neural networks with multiple hidden layers to learn from data. With the complex nonlinear structure, deep learning can effectively adopt model fitting to accelerate the design process without continuously transferring data in each design step.¹³ Currently, deep learning has been applied in various areas such as computer vision and natural language processing.¹⁴ In the meantime, deep learning, as a powerful computational technique, has emerged as an effective tool for feature learning in photonics. Research in this field has been conducted with respect to various photonic applications, including unique shape design of metasurfaces,¹⁵⁻¹⁹ structure prediction in photonic crystals,^{13,20} and inverse design of nanophotonic structures.^{21,22} To date, deep learning has yet to be incorporated into structure design of a WLED for improving ACU and luminous flux simultaneously. Such task of inverse design is complex and finding the optimized design can be beyond human capabilities when multiple parameters need to be considered for optimization. Although deep learning offers a promising solution to this complex task, how to develop a neural network model and the corresponding learning process for CNC nanocomposite film design still requires extensive research.

The typical model architectures in deep learning are deep neural networks (DNN),²³ convolutional neural networks, recurrent neural networks, and deep generative models. In literature, the convolutional neural network has been used for the photonic problem like

nonlinear electromagnetic inverse scattering with images as inputs because this deep model can extract the features of high-dimensional inputs with convolution operations.²⁴ Besides, previous research applies the recurrent neural network capable of learning sequence data to analyze optical signals and noises in high-speed fiber transmission.²⁵ As one popular branch of deep generative models, generative adversarial networks can generate results similar to the training dataset. This network has been used for realizing high efficiency in the inverse design of metasurfaces with training images as inputs.¹⁵ However, in this study, CNC nanocomposite films are constructed by structural parameters according to the on-demand figure-of-merits. Convolution operations will face obstacles in capturing spatial information for the low-dimensional features. Deep generative models are inapplicable for this regression problem. Additionally, the input features are the disordered parameter sets that are unnecessary to perform recursion in the evolution direction of the sequence. It indicates that recurrent neural networks are inappropriate to be used in building the inverse design architecture for this study. Some recent research works indicate that DNN is well suited for the reverse design of structural parameters for optical structures, such as inverse design H-shape metallic structures.²⁶ DNN is capable of fitting continuous functions for the features because it contains multiple hidden layers with sufficient hidden units allowing it to model complicated input-output relationships according to the universal approximation theorem.²⁷ With the multilayered architecture, DNN has benefits in learning the hierarchical representations and a nonlinear transformation of the input features. In this paper, we apply DNN to learn the structural features and inverse design of the CNC nanocomposite films on the WLED optical module.

Here, we focus on the design of CNC nanocomposite film that covers on the WLED module to improve both figure-of-merits: ACU and luminous flux. We propose a new approach to strengthen the integrated performances (luminous flux and ACU) of WLEDs by training a tandem deep neural network (DNN) to address the nonuniqueness issue existing in the inverse design.²² CNC

nanocomposite films of different structural parameters can provide similar figure-of-merits, which leads to the nonunique mapping between inputs and outputs. It consequently results in nonuniqueness problems, and the networks meet the failure of convergence during the training process.²⁸ This study presents our method of training the bidirectional DNN model in the inverse design. In the forward DNN model, the inputs are the parameters representing the CNC nanocomposite film structures, and the two performances (luminous flux and ACU) are the outputs. An inverse predicting network based on an inverse DNN model and a pretrained forward DNN model generates the variables to form structures corresponding to various performance sets to form tandem architecture. Consequently, this deep learning model can not only predict two performances with high accuracy in the forward direction (mean square error at 6.55×10^{-3}) but also generate valid parameters of CNC nanocomposite films covering WLEDs in inverse design. Through deep learning prediction and verified simulations, we locate several parameters to construct the structures of CNC nanocomposite film in the WLEDs module with higher luminous flux and ACU simultaneously. Furthermore, this deep learning approach provides solutions that are much faster and more productive than the conventional methods for demands of performances.

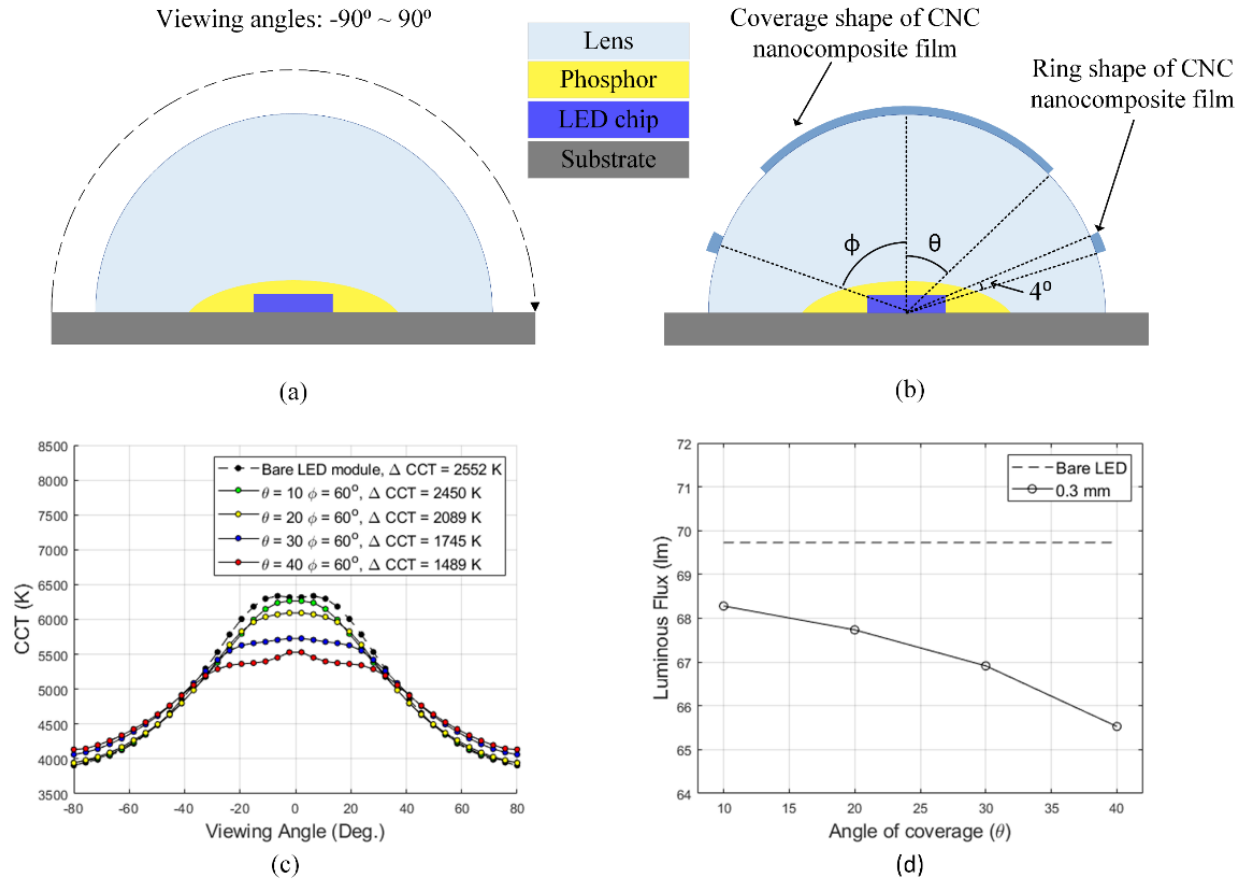


Figure 2-1: (a) Bare WLED packaging module. (b) luminous flux and ACU optimization by coating the WLED module with coverage and a ring shape, where θ is the angle of coverage, and ϕ is the angle of the ring shape. (c) Angular CCT of WLED module with various coverage angles based on ring angle ($\phi = 60^\circ$), the concentration of 4 wt.%, and film thickness of 0.3 mm. (d) Luminous flux as a function of angle of coverage.

2.2 Data collection

2.2.1 Simulation methods

The structure of common phosphor-converted WLEDs has been discussed and constructed in previous studies.^{29,30} Commercial simulation software Zemax OpticStudio was used in this work. Fig. 2-1(a) shows the optical model of a WLED module used in simulations, in which the size of the LED chip is $1 \times 1 \text{ mm}^2$, with a layered stack consisting of p-GaN, multi-quantum well (MQW), n-GaN, sapphire substrate, and metal alloy film. The thicknesses of each layer are 150 nm, 100

nm, 4 μm , 140 μm , and 0.1 μm , respectively. The LED chip is covered by the dispensing-coated phosphor-silicone layer. These structures are inside a hemisphere silicone lens with a radius of 3 mm. The material and optical properties of CNC have been described in the previous work.³¹ The particle size of the nanocrystal used in the simulation is 3 μm . According to our previous publication,¹¹ slight variations in CNC particle size and uniformity of CNC dispersion have little influence on the optical properties of the nanocomposite film. As a comparison, Fig. 2-1(b) displays a new WLED module structure with the CNC nanocomposite film as an optical diffuser, which is divided into top coverage (θ) and side surrounding ring (ϕ). The arc measure for the surrounding ring is fixed at 4° to allow sufficient variations according to each coverage angle (θ) and generating noticeable changes for figure-of merits. When we optimized our nanocomposite films, we found that the central coverage of CNC nanocomposite film can improve Δ CCT but decrease the luminous flux. However, a side ring nanocomposite film at different angles could give better luminous flux when maintain the Δ CCT. Thus, we used the combination of a central coverage and a side ring nanocomposite film for design optimization. The detector in the simulation was set to capture the light from the integrated WLED module in the range of viewing angles from -90 deg to 90 deg (Fig. 2-1(a)). By increasing the angle of top coverage (θ) in the optical simulations, Fig. 2-1(c) and Fig. 2-1(d) demonstrate that correlated color temperature deviation (Δ CCT) is lowered, representing an improvement of ACU, but luminous flux decreases.

2.2.2 Original data collection

To realize the deep learning approach and address the targets described above, we varied four parameters and characterized the resulting luminous flux and Δ CCT; parameters include the two angles (ϕ and θ) for CNC nanocomposite film, CNC concentration (weight percentage wt.%) and film thickness. Fig. 2-2(a) shows the result for the rise of concentration, which illustrates that more quantity of CNC particles in the polymer will decrease luminous flux but improve ACU. Furthermore, the increase of thickness and top coverage (θ) describes radial and tangential

growth of CNC nanocomposite film respectively on the lens. As shown in Fig. 2-2(b) and Fig. 2-2(c), the uniformity of CCT and luminous flux improves and falls respectively through the rise of thickness and coverage angle due to an increase in the total quantity of CNC nanocomposite film used. Fig. 2-2(d) indicates that increasing angle of CNC nanocomposite ring does not necessarily increase/decrease ACU and luminous flux. The defined parameters are in the intervals that include ample samples covering enough amplitude of performances. The concentration is tuned from 0.5 to 4 wt.%, and the thickness is changed from 0.1 to 0.3 mm with step sizes of 0.5 and 0.1, respectively. In order to ensure the presence of the ring nanocomposite, the ring angle (ϕ) should be at least 10 degrees larger than the coverage shape angle (θ), and both angles are less than 90 degrees to be able to cover the lens. To construct the original data set, the four parameters are combined to generate various structures and obtain their performances in simulations. It is also noted that Δ CCT and luminous flux increase or decrease at the same time in the simulated results. Thus, for improving ACU and luminous flux simultaneously, finding optimized four parameters to lower Δ CCT while keeping high luminous flux is a challenging task. Here we developed forward predicting architecture and reverse network design to address this challenge.

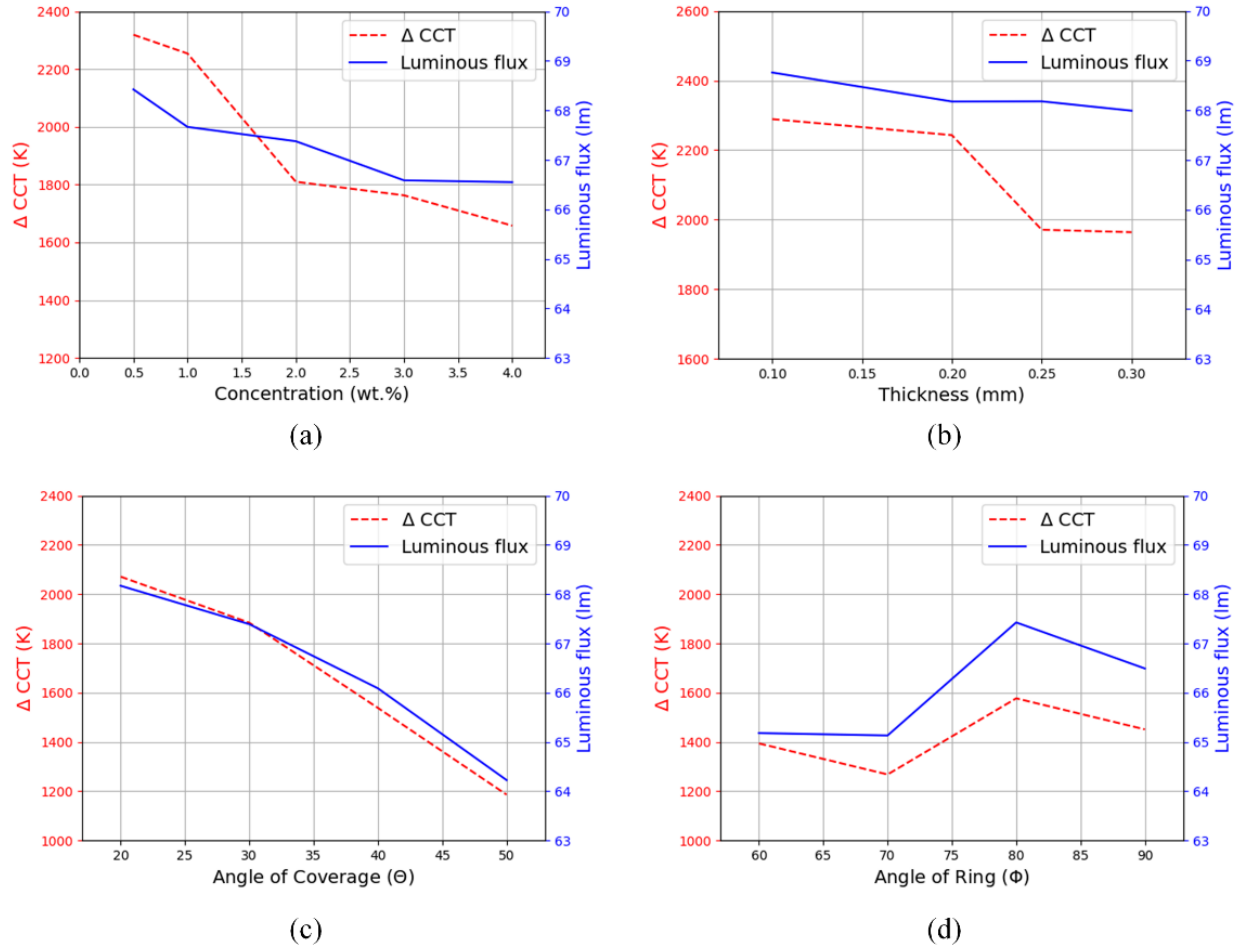


Figure 2-2: Variation of simulated results of Δ CCT (red dashed line) and luminous flux (blue line) according to each parameter: (a) Concentration. Fixed parameters are coverage ($\theta = 40^\circ$) and ring ($\phi = 70^\circ$) shapes with a thickness of 0.3 mm. (b) Thickness. Fixed parameters are coverage ($\phi = 70^\circ$) and ring ($\phi = 50^\circ$) shapes with 4 wt.% concentration. (c) The angle of coverage. Fixed parameters are the ring angle ($\phi = 65^\circ$) with concentration and thickness of 4 wt.% and 0.3 mm, respectively. (d) The angle of the ring shape. Fixed parameters are the coverage ($\theta = 50^\circ$) shape with 4 wt.% concentration and 0.2 mm thickness.

2.3 Inverse design methodology

The workflow to design the reverse network is shown in Fig. 2-3, in which the inverse predicting network is set as the primary process to find unique parameter sets and the pretrained forward network is used to assist with learning and optimizing. The overall reverse design using deep learning can be divided into four phases: original data collection, training forward predicting

model, inverse network design, and sampling-based search for the best performance. The first phase is to use simulation to create the original data containing the structural parameters corresponding to their figure-of-merits, as discussed above. In the second phase, we build a forward DNN model with structural parameters and performances as input and output, respectively. This forward predicting model is trained by applying the training set of the original data set to learn and optimize model weights. When the model reaches convergence and achieves high accuracy without overfitting, it meets the goals of pretrained forward DNN and can be used to solve the nonuniqueness problem. The inverse network design phase (third phase) involves an inverse DNN and the pretrained forward DNN model. In the inverse DNN model, the input is the randomly selected figure-of-merits within a reasonable range, and the output is limited by passing through the nonlinear constraint layer. Thus, the generated parameters as input are received by pretrained forward DNN architecture and the model then calculates output parameters. The inverse predicting model is able to learn the inner set of rules of the structural parameters and figure-of-merits by comparing the output and initial performances. The final phase is to sampling-search the improved figure-of-merits according to the structural parameter sets produced by the inverse predicting model.

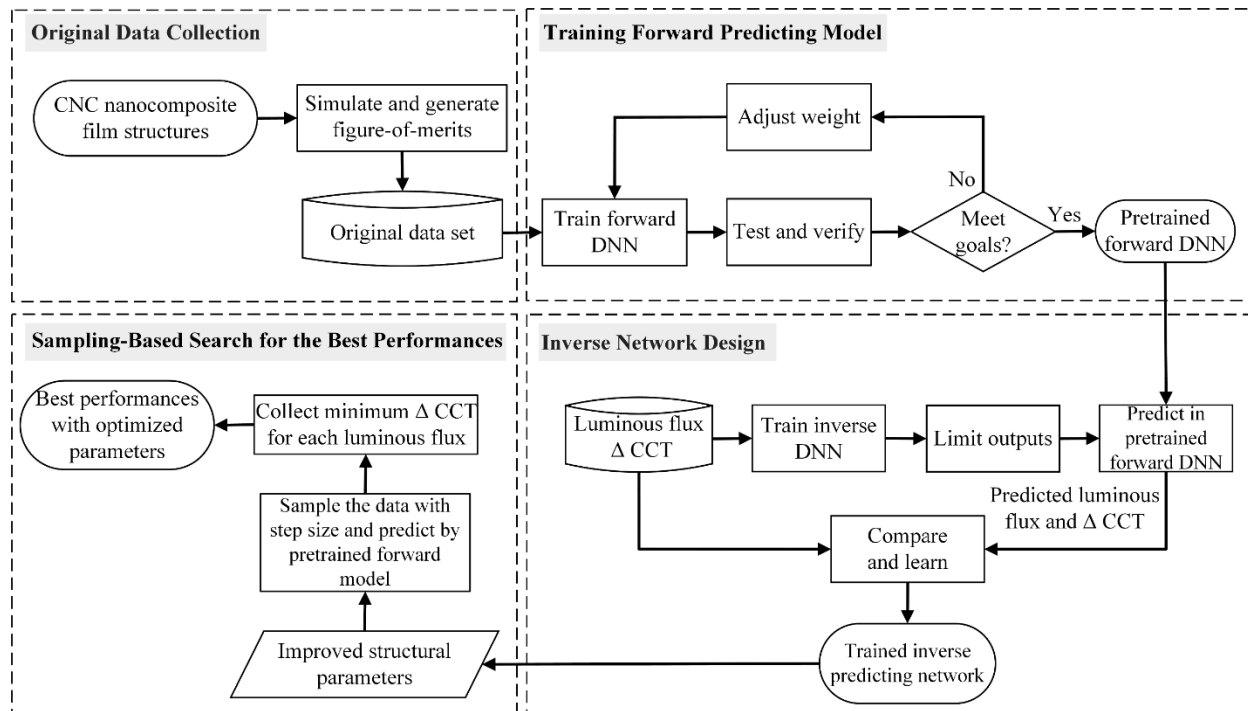


Figure 2-3: Flowchart of the entire design scheme using deep learning approach.

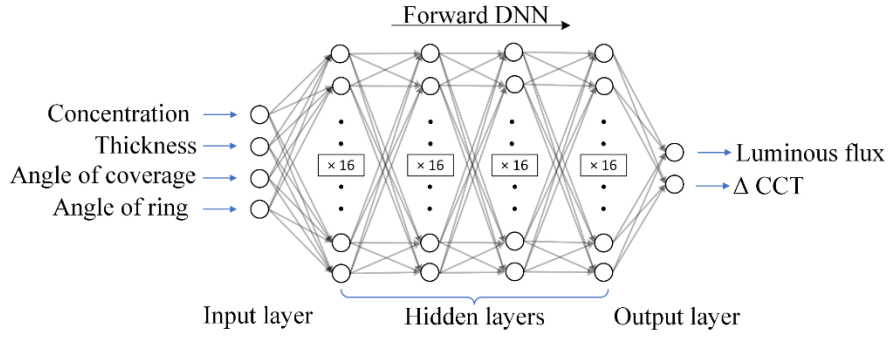
2.4 Results and discussion

2.4.1 Forward predicting architecture and model evaluation

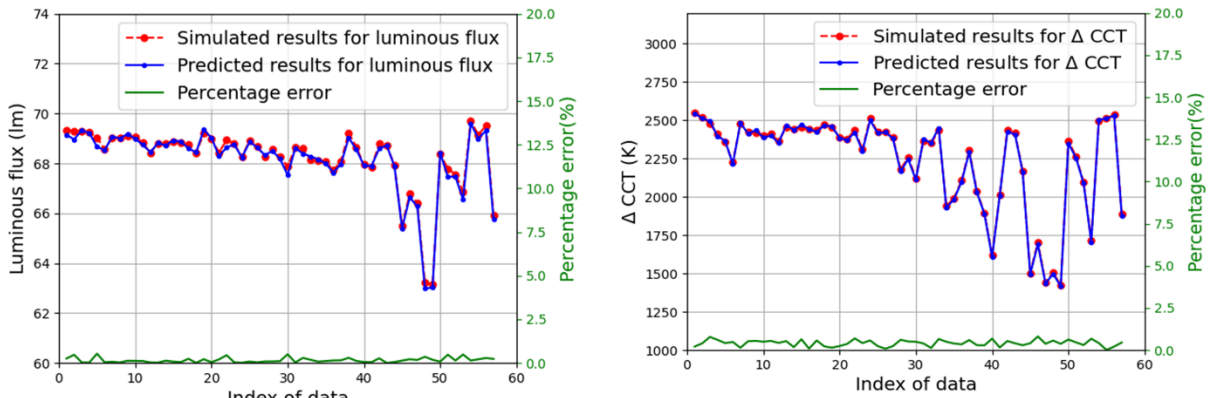
As shown in Fig. 2-4(a), we built the forward DNN model that consists of 6 fully connected layers, in which the first 5 layers are each followed by an ReLU activation function. As the first layer of this network, the input layer has 4 neurons according to the parameters. Each of the 4 hidden layers contains 16 neurons, and the final layer is the output layer with 2 neurons corresponding to luminous flux and Δ CCT. The forward DNN model can fit the relationship between the structural parameters and the two figure-of-merits, and the target of developing this model is to use it in the design process and accelerate the design flow by substituting the simulation methods with this model. In the original data collection, we varied the values of four structure parameters, and performed simulation to obtain 160 samples of CNC structures and their figure-of-merits. For

developing the forward neural network, 80% (128 sets) and 20% (32 sets) of the total input sets were used as training sets and validation sets.

The forward DNN model was implemented in PyTorch and optimized using the stochastic gradient descent optimizer. To guarantee productive learning with gradient descent algorithms, all the features in the original data set were individually normalized. The network was trained by minimizing mean squared error as a loss function. After training for a total of 10000 epochs, the forward DNN model achieved mean squared errors of 6.55×10^{-3} and 6.56×10^{-3} for the training and validation sets, respectively. These small mean squared errors ensure the high accuracy (low percentage error) in predicting figure-of-merits of WLEDs as shown in Fig. 2-4. To further show that our forward network is well pretrained, Fig. 2-4(b) compares the predictions of the forward DNN model with original simulated values of two performances for the training set. The predicted phase almost perfectly overlaps simulation results. The percentage errors between the predictions and simulations in both figures are consistently lower than 1%. Overall, the forward DNN model can be applied to replace the conventional optical simulations used to generate the two performances. Moreover, each simulation for a new design in the original data set takes at least 45 minutes, consisting of creating the model, a one ray tracing simulation, and related numerical calculations. In contrast, the pretrained forward DNN model can calculate the two performances of a set of designs within a few seconds by using the same computing system. Thus, the forward DNN model has the ability to save a large quantity of time and effort. Equally important, this well pretrained network establishes the foundation for building an inverse predicting model, requiring the forward DNN model to behave remarkably in predicting the two performances.



(a)



(b)

Figure 2-4: (a) Forward neural network consisted of fully connected DNN. This forward predicting model takes concentrations, thickness, angle of coverage, and ring shape angle of CNC nanocomposite films as inputs and generates luminous flux and Δ CCT. (b) Comparison of simulated (red dotted dashed line) and predicted (blue dotted line) luminous flux and Δ CCT of samples in the normalized training set. The percentage error (green line) is the absolute difference between simulations and predictions in percentage.

2.4.2 Inverse network design

In a typical scenario, an optical designer creates a WLED module with an optical diffuser meeting the required performances and needs to discover the optimized structures to realize the better performances in terms of lower Δ CCT and higher luminous flux. The traditional design procedure is to continuously change certain parameters relying on experiences and physical intuition. As we presented above, an inverse DNN model can solve this problem by using Δ CCT and luminous flux as two inputs to predict four parameters. However, two critical obstacles need to be addressed when the parameters and performances are implemented in this conventional DNN model. One

fundamental problem is that various parameter sets can achieve the same performances, which leads to the nonuniqueness problem in the DNN training process. To solve it, we built an inverse predicting architecture using the tandem network in which an inverse DNN model is connected to the pretrained forward DNN model. Secondly, the whole network should satisfy the relationships of two angles as discussed above in the process of learning and converging. Thus the model can provide the parameters with actual physical meaning to define the structures. To this end, we added one nonlinear restriction layer after the inverse DNN model. Eventually, this pretrained inverse network can be used to output one parameter set achieving the desired performances and discovering new features to realize optimization. For the first part of this inverse predicting model, A fully connected network set to four layers with each layer having 2-8-8-4 neurons can be functional. A ReLU activation function follows the input layer and each hidden layer. The two random performances in the reasonable ranges are fed as the inputs of the inverse DNN model, and four variables are calculated as the intermediate results serving as an input to the next layer. To build the nonlinear constraints layer, we first assigned a Sigmoid activation function after the output layer of inverse architecture to limit the values that the network can generate between 0 and 1. These results then passed through two linear functions (Eq. 1) to complete and realize the target, followed by re-normalization and transmitted to the forward DNN model as inputs. The outputs from the nonlinear constraint layer can effectively range the parameters and propagate to the next phase.

$$\phi_i = 10 + 80 * \phi_s, \theta_i = (\phi_i - 10) * \theta_s \quad (1)$$

The modified inverse predicting model can effectively learn the comparison between the figure-of-merits corresponding to the output structural parameters from the constraint layer and the initial performance with the assistance of the pretrained forward network. The structural parameters as intermediate values can be obtained as the result of the inverse design. Fig. 2-5(a) shows the integrated inverse design network. To train this tandem DNN model, we uniformly and randomly generated the two performances for 200 input sets within the ranges ([64, 69] for

luminous flux and [1000, 2500] for Δ CCT). The maximum and minimum values for the ranges are the performances of the bare WLED module and its lens thoroughly coated with CNC nanocomposite film. Thus, these input sets can effectively cover the ranges of the two performances and ensure the differences between each input set. In order to obtain a good inverse network, 10,000 iterations were carried out for each input set so that all neutrals can be appropriately linked in the inverse DNN. As shown in Fig. 2-5(b), the percentage errors are lower than 8% for all input sets. During the training process of the whole network, the weights of pretrained forward networks are fixed, and we use a stochastic gradient descent optimizer to minimize the mean square error as the cost function. The mean square error of this inverse predicting DNN model is stably located at 0.3 after converging. Corresponding to various input sets, this inverse network generates parameter sets that are all valid and physically meaningful values. In order to verify the actual responses of the predicted features, we implemented them into the simulations to generate the compared results. As seen in Fig. 2-5(b), the simulated performances of parameter sets predicted from the inverse predicting model are close to the target values. These results provide confidence in utilizing deep learning methods to inversely design structures of optical diffusers within the WLEDs module to reach improved performances.

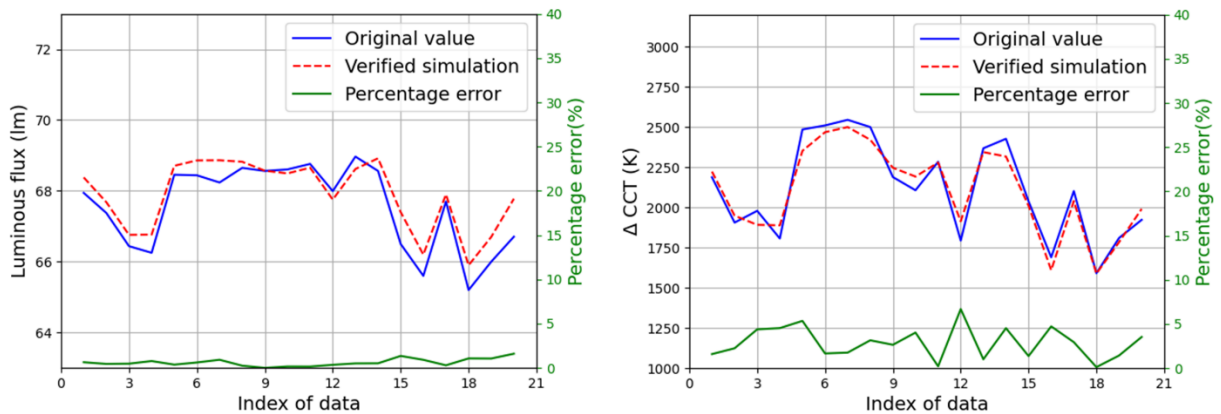
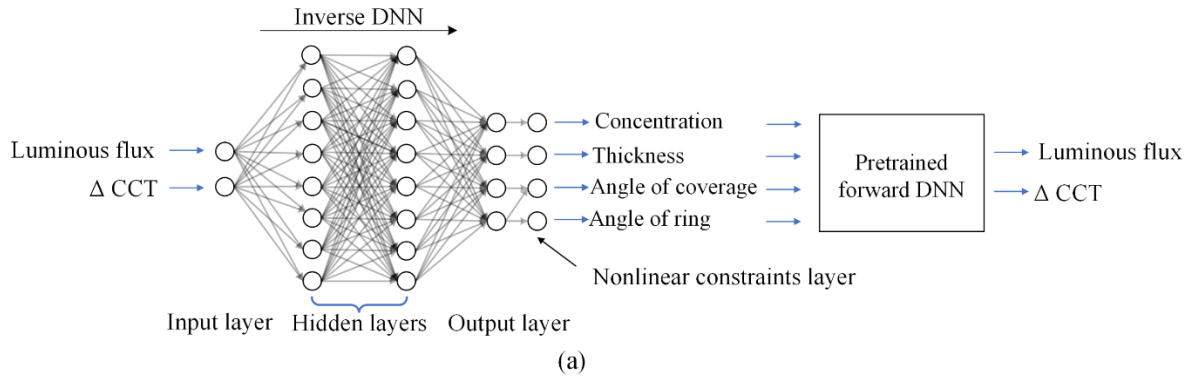


Figure 2-5: (a) Inverse predicting tandem architecture formed with DNN-based inverse neural network, nonlinear constraints layer, and pretrained forward DNN model. The inputs and outputs of this network are both luminous flux and Δ CCT. (b) The evaluation of the inverse predicting tandem model for 20 random combinations of the two performances shows the differences between target performance sets (blue line) and verified simulations (red dashed line) based on predicted parameters.

2.4.3 Sampling-based search for the best performances

Although the inverse prediction network successfully predicts the parameters for the target figure-of-merits, we expect the deep learning method in this study to discover new designs to enhance the two performances of WLEDs simultaneously.

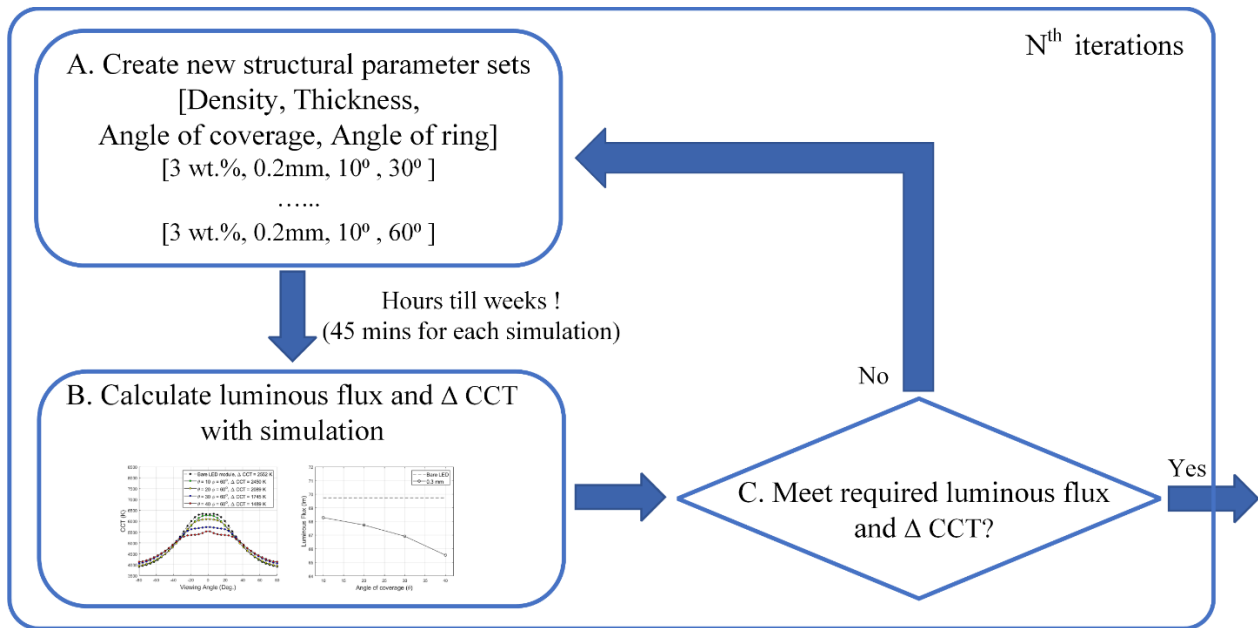


Figure 2-6: Workflow of the common method to search the performances. (A) Create diverse sets of structural parameters. (B) Simulate the luminous flux and Δ CCT for each parameter set. (C) Check the simulated results with the required figure-of-merits. This approach needs to iterate these steps before meeting the goals and enormous simulations are time-consuming.

To search for the best performances that our WLED module can achieve, the common method shown in Fig. 2-6 is to traverse all the possible combinations of the two figure-of-merits into simulation software to calculate the answers and compare to locate the required performances.³² However, it is difficult and time-consuming to traverse each decimal precision of values and requires plenty of verified simulations.

Fig. 2-7(a) shows the scatter plot of the performances in the original data set used for training the forward DNN model, and the red dash line represents data with the best performance (low Δ CCT and high luminous flux achieved at the same time) in the original data set. To find structure parameters that can lead to better performance than the ones showing on the red dash line, we applied our inverse DNN to find structure parameters according to a set of given figure-of-merits (performance). Compared to the common method, we took a group of inputs by continuously reducing Δ CCT with a step size of 100 for one luminous flux in the same range as in the original

data set. Since the inverse model has fully converged, it can be used to search and locate the parameter sets for improved figure-of-merits with rough precisions. After verified simulations, we obtained new structures that realize better ACU for each luminous flux, as shown in the blue solid line of Fig. 2-7(b). Our method of finding improved performances by using inverse DNN successfully solves the issue of time-consuming in the common method. Comparing the blue solid line to the red dash line, we have realized a reduction of 100-200 in Δ CCT corresponding to the total range of luminous flux.

Our target is to find exact values of the best performances and their structural parameter sets with high precision. To realize them, we sampled all combinations of the four parameters nearby the improved results (blue solid line in Fig. 2-7(b)) generated from the inverse model in the previous step. The ranges and step sizes of values for each of these four parameters are shown in Table 1. For more effective use of developed forward predicting architecture, we further applied the pretrained forward DNN model in the range around each parameter to search for better performance. This further optimization using the forward predicting architecture can greatly reduce the time required for optimization while keeping the accuracy in forward prediction. Fig. 2-7(c) shows the schematic of the traversing search with the pretrained forward DNN model. Following simulations verified the outputs from the forward DNN model. Thus, optimized fine-tuning results are shown as green dots in Fig. 2-7(b). It shows that the designed inverse model successfully gives a specific optimization direction. Fig. 2-7(d) shows two examples of the new designs of coverage and the ring shape of CNC nanocomposite films from optimization results, which indicates the unique combinations of parameter sets that are difficult to find in the manual design flow. The common method takes 45 minutes for one simulation and completing the optimization will require thousands of simulations in iterations to find the four structure parameters. Compared to the common method, this demonstrated work only requires a few milliseconds using the trained inverse DNN and forward DNN models.

Table 2-1. Ranges and step sizes of concentration, thickness, angle of coverage, and angle of the ring shape.

<i>Parameters</i>	<i>Step size</i>	<i>Range</i>
<i>Concentration (wt.%)</i>	<i>0.100</i>	<i>± 0.300</i>
<i>Thickness (mm)</i>	<i>0.020</i>	<i>± 0.060</i>
<i>Angle of coverage (θ)</i>	<i>2.000</i>	<i>± 6.000</i>
<i>Angle of the ring shape (ϕ)</i>	<i>2.000</i>	<i>± 6.000</i>

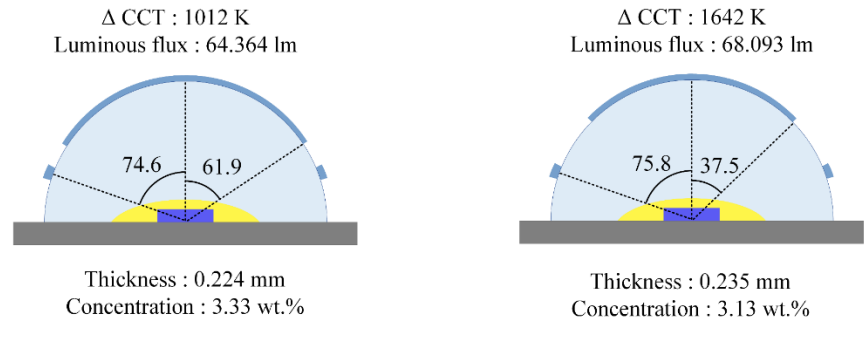
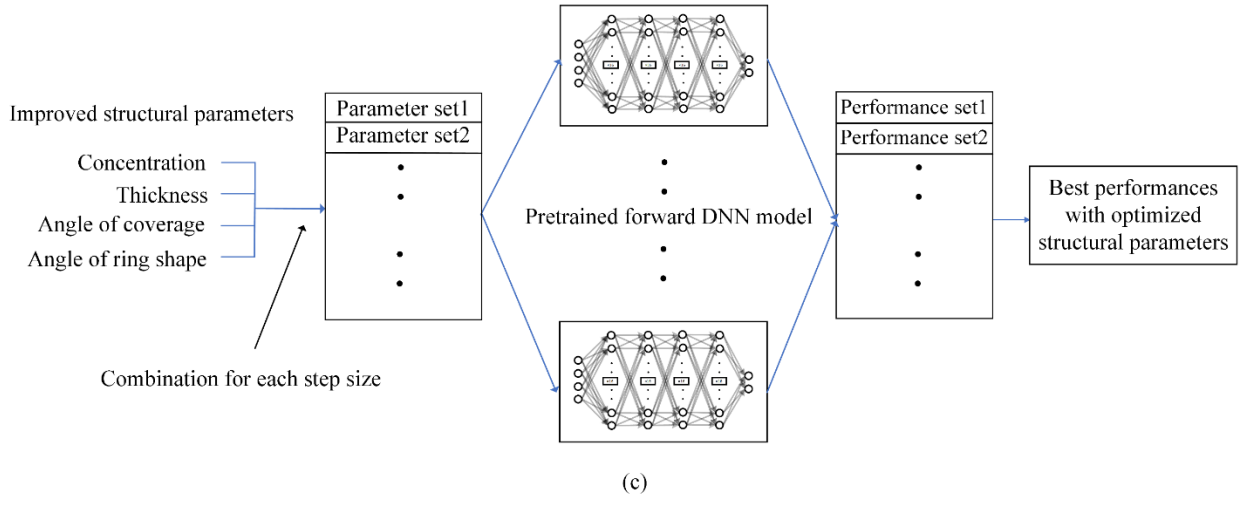
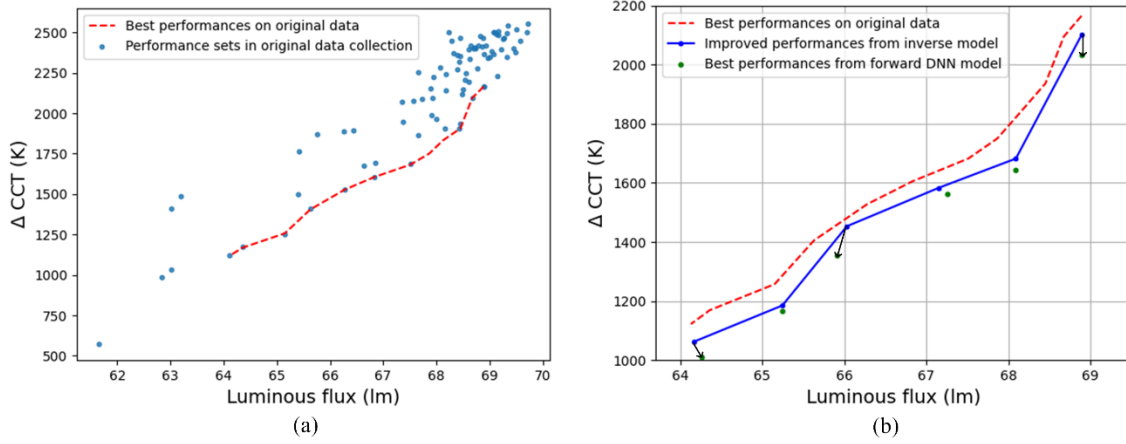


Figure 2- 7: (a) The performance sets of the original data set used in the forward DNN model. (b) Comparison of the best performance sets in the original data set (red dashed line), improved performance (blue line) predicted from the inverse predicting model, and enhanced performances (green dots) by sampling searching with the forward DNN model. (c) Schematic of sampling-based search using pretrained forward DNN model. (d) Visualization of the structures of CNC nanocomposite layers based on two optimized parameter sets.

2.5 Conclusion

In conclusion, we proposed a DNN-based data-driven method for rapid and accurate inverse design of two geometries of CNC nanocomposite film on WLED modules. The iterative workflow of inverse design in building the structures of optical diffusers can be simplified by using an inverse predicting network to generate desired structure. By combining the inverse predicting model and the forward propagation network, we located new parameter sets and realized optimized figure-of-merits. These results further provide a solution for the fast inverse design of optical diffusers with various shapes and materials on WLED modules. Although this paper mainly discussed the inverse design of a planar structure, the presented method can be extended to three-dimensional geometry in the future work by introducing more structural features according to different figure-of-merits.

Reference

- (1) Pust, P.; Schmidt, P. J.; Schnick, W. A Revolution in Lighting. *Nature Materials*. Nature Publishing Group May 1, **2015**, pp 454–458. <https://doi.org/10.1038/nmat4270>.
- (2) van de Haar, M. A.; Tachikirt, M.; Berends, A. C.; Krames, M. R.; Meijerink, A.; Rabouw, F. T. Saturation Mechanisms in Common LED Phosphors. *ACS Photonics* **2021**, *8* (6), 1784–1793. <https://doi.org/10.1021/acsp Photonics.1c00372>.
- (3) Cho, J.; Park, J. H.; Kim, J. K.; Schubert, E. F. White Light-Emitting Diodes: History, Progress, and Future. *Laser and Photonics Reviews*. Wiley-VCH Verlag March 1, **2017**. <https://doi.org/10.1002/lpor.201600147>.
- (4) Liu, Z. Y.; Li, C.; Yu, B. H.; Wang, Y. H.; Niu, H. ben. Effects of YAG: Ce Phosphor Particle Size on Luminous Flux and Angular Color Uniformity of Phosphor-Converted White LEDs. *IEEE/OSA Journal of Display Technology* **2012**, *8* (6), 329–335. <https://doi.org/10.1109/JDT.2012.2184835>.
- (5) Chowdhury, F. I.; Xu, Q.; Wang, X. Improving the Light Quality of White Light-Emitting Diodes Using Cellulose Nanocrystal-Filled Phosphors. *Adv Photonics Res* **2021**, *2* (5), 2100006. <https://doi.org/10.1002/adpr.202100006>.
- (6) Wang, P. C.; Su, Y. K.; Lin, C. L.; Huang, G. S. Improving Performance and Reducing Amount of Phosphor Required in Packaging of White LEDs With TiO₂-Doped Silicone. *IEEE Electron Device Letters* **2014**, *35* (6), 657–659. <https://doi.org/10.1109/LED.2014.2318037>.
- (7) Chen, K. J.; Han, H. V.; Lin, B. C.; Chen, H. C.; Shih, M. H.; Chien, S. H.; Wang, K. Y.; Tsai, H. H.; Yu, P.; Lee, P. T.; Lin, C. C.; Kuo, H. C. Improving the Angular Color Uniformity of Hybrid Phosphor Structures in White Light-Emitting Diodes. *IEEE Electron Device Letters* **2013**, *34* (10), 1280–1282. <https://doi.org/10.1109/LED.2013.2278336>.
- (8) Wang, K.; Wu, D.; Chen, F.; Liu, Z.; Lu, X.; Liu, S. Freeform Lens for White LEDs with High Angular Color Uniformity. In *Electronics System Integration Technology Conference, ESTC 2010 - Proceedings*; **2010**. <https://doi.org/10.1109/ESTC.2010.5642939>.
- (9) Zheng, H.; Luo, X. Color Consistency Enhancement of White Light-Emitting Diodes through Substrate Design. *IEEE Photonics Technology Letters* **2013**, *25* (5), 484–487. <https://doi.org/10.1109/LPT.2013.2241756>.
- (10) Xu, Q.; Meng, L.; Wang, X. Nanocrystal-Filled Polymer for Improving Angular Color Uniformity of Phosphor-Converted White LEDs. *Appl Opt* **2019**, *58* (27), 7649. <https://doi.org/10.1364/ao.58.007649>.
- (11) Mahpeykar, S. M.; Zhao, Y.; Li, X.; Yang, Z.; Xu, Q.; Lu, Z. H.; Sargent, E. H.; Wang, X. Cellulose Nanocrystal:Polymer Hybrid Optical Diffusers for Index-Matching-Free Light Management in Optoelectronic Devices. *Adv Opt Mater* **2017**, *5* (21). <https://doi.org/10.1002/adom.201700430>.

- (12) Zhou, L.; Xiao, Y.; Chen, W. Machine-Learning Attacks on Interference-Based Optical Encryption: Experimental Demonstration. *Opt Express* **2019**, *27* (18), 26143. <https://doi.org/10.1364/oe.27.026143>.
- (13) Asano, T.; Noda, S. Optimization of Photonic Crystal Nanocavities Based on Deep Learning. *Opt Express* **2018**, *26* (25), 32704. <https://doi.org/10.1364/oe.26.032704>.
- (14) Zhang, T.; Liu, Q.; Dan, Y.; Yu, S.; Han, X.; Dai, J.; Xu, K. Machine Learning and Evolutionary Algorithm Studies of Graphene Metamaterials for Optimized Plasmon-Induced Transparency. *Opt Express* **2020**, *28* (13), 18899. <https://doi.org/10.1364/oe.389231>.
- (15) Liu, Z.; Zhu, D.; Rodrigues, S. P.; Lee, K. T.; Cai, W. Generative Model for the Inverse Design of Metasurfaces. *Nano Lett* **2018**, *18* (10), 6570–6576. <https://doi.org/10.1021/acs.nanolett.8b03171>.
- (16) Liao, X.; Gui, L.; Yu, Z.; Zhang, T.; Xu, K. Deep Learning for the Design of 3D Chiral Plasmonic Metasurfaces. *Opt Mater Express* **2022**, *12* (2), 758. <https://doi.org/10.1364/ome.449152>.
- (17) Roberts, N. B.; Keshavarz Hedayati, M. A Deep Learning Approach to the Forward Prediction and Inverse Design of Plasmonic Metasurface Structural Color. *Appl Phys Lett* **2021**, *119* (6). <https://doi.org/10.1063/5.0055733>.
- (18) Nadell, C. C.; Huang, B.; Malof, J. M.; Padilla, W. J. Deep Learning for Accelerated All-Dielectric Metasurface Design. *Opt Express* **2019**, *27* (20), 27523. <https://doi.org/10.1364/oe.27.027523>.
- (19) Tanriover, I.; Hadibrata, W.; Aydin, K. Physics-Based Approach for a Neural Networks Enabled Design of All-Dielectric Metasurfaces. *ACS Photonics* **2020**, *7* (8), 1957–1964. <https://doi.org/10.1021/acsp Photonics.0c00663>.
- (20) Wu, J.; Li, J.; Liu, X.; Gong, L.; Chen, J.; Tang, Z.; Lin, W.; Mu, Y.; Lin, X.; Hong, W.; Yi, G.; Chen, X. Unclonable Photonic Crystal Hydrogels with Controllable Encoding Capacity for Anticounterfeiting. *ACS Appl Mater Interfaces* **2022**, *14* (1), 2369–2380. <https://doi.org/10.1021/acsam.1c20905>.
- (21) Wiecha, P. R.; Muskens, O. L. Deep Learning Meets Nanophotonics: A Generalized Accurate Predictor for near Fields and Far Fields of Arbitrary 3D Nanostructures. *Nano Lett* **2020**, *20* (1), 329–338. <https://doi.org/10.1021/acs.nanolett.9b03971>.
- (22) Liu, D.; Tan, Y.; Khoram, E.; Yu, Z. Training Deep Neural Networks for the Inverse Design of Nanophotonic Structures. *ACS Photonics* **2018**, *5* (4), 1365–1369. <https://doi.org/10.1021/acsp Photonics.7b01377>.
- (23) Ma, W.; Liu, Z.; Kudyshev, Z. A.; Boltasseva, A.; Cai, W.; Liu, Y. Deep Learning for the Design of Photonic Structures. *Nature Photonics*. Nature Research February 1, 2021, pp 77–90. <https://doi.org/10.1038/s41566-020-0685-y>.
- (24) Li, L.; Wang, L. G.; Teixeira, F. L.; Liu, C.; Nehorai, A.; Cui, T. J. DeepNIS: Deep Neural Network for Nonlinear Electromagnetic Inverse Scattering. *IEEE Trans Antennas Propag* **2019**, *67* (3), 1819–1825. <https://doi.org/10.1109/TAP.2018.2885437>.

- (25) Zhou, Q.; Yang, C.; Liang, A.; Zheng, X.; Chen, Z. Low Computationally Complex Recurrent Neural Network for High Speed Optical Fiber Transmission. *Opt Commun* **2019**, *441*, 121–126. <https://doi.org/10.1016/j.optcom.2019.02.037>.
- (26) Malkiel, I.; Mrejen, M.; Nagler, A.; Arieli, U.; Wolf, L.; Suchowski, H. Plasmonic Nanostructure Design and Characterization via Deep Learning. *Light Sci Appl* **2018**, *7* (1). <https://doi.org/10.1038/s41377-018-0060-7>.
- (27) Liu, C. X.; Yu, G. L.; Zhao, G. Y. Neural Networks for Inverse Design of Phononic Crystals. *AIP Adv* **2019**, *9* (8). <https://doi.org/10.1063/1.5114643>.
- (28) Wu, Q.; Li, X.; Wang, W.; Dong, Q.; Xiao, Y.; Cao, X.; Wang, L.; Gao, L. Comparison of Different Neural Network Architectures for Plasmonic Inverse Design. *ACS Omega* **2021**, *6* (36), 23076–23082. <https://doi.org/10.1021/acsomega.1c02165>.
- (29) Zheng, H.; Wang, Y.; Li, L.; Fu, X.; Zou, Y.; Luo, X. Dip-Transfer Phosphor Coating on Designed Substrate Structure for High Angular Color Uniformity of White Light Emitting Diodes with Conventional Chips. *Opt Express* **2013**, *21* (S6), A933. <https://doi.org/10.1364/oe.21.00a933>.
- (30) Wang, S.; Chen, X.; Chen, M.; Zheng, H.; Yang, H.; Liu, S. Improvement in Angular Color Uniformity of White Light-Emitting Diodes Using Screen-Printed Multilayer Phosphor-in-Glass. *Appl Opt* **2014**, *53* (36), 8492. <https://doi.org/10.1364/ao.53.008492>.
- (31) Xu, Q.; Meng, L.; Wang, X. Reducing Shadowing Losses in Silicon Solar Cells Using Cellulose Nanocrystal: Polymer Hybrid Diffusers. *Appl Opt* **2019**, *58* (10), 2505. <https://doi.org/10.1364/ao.58.002505>.
- (32) Paradiso, S. P.; Delaney, K. T.; Fredrickson, G. H. Swarm Intelligence Platform for Multiblock Polymer Inverse Formulation Design. *ACS Macro Lett* **2016**, *5* (8), 972–976. <https://doi.org/10.1021/acsmacrolett.6b00494>.

Chapter 3. Scattering optics for LED lighting achieved by nanocrystals and machine learning

3.1. Introduction

Optical design was synonymous with the design of imaging optics in the past.¹ While white LEDs (WLEDs) become the major light sources for the world, non-imaging optics, especially illumination design, started to emerge as an important area of engineering practice to optimize LED lighting systems for various practical applications.² For efficient transfer of light from the source to the target, two major parameters are required to be considered in illumination design: transfer efficiency and the distribution at the target.³ For improving the transfer efficiency in illumination design of WLED sources, various techniques have been employed to boost the overall brightness (luminous flux) from WLEDs.^{3,4} In order to control the distribution of light as the target, lenses and mirrors are applied to change the spatial distribution of WLED light (brightness distribution), and the emerging field of freeform optics has been established to produce desired brightness patterns using specially designed lens shape and size^{3,4}. Although scattering optics (i.e. optics diffusers), has been applied to improve the overall brightness of WLEDs⁵, it has never been demonstrated to achieve desired brightness distribution. It is generally believed that lack of control in transferring light in space makes optical diffusers impossible to focus light onto desired directions, so producing complex brightness distribution (patterns) using optical diffusers by the brute force approach (searching through all possible choices) is beyond the capacity of typical optics designers.

Machine learning, which is famous for making predictions better than humans, has been applied for inverse design of photonic structures for broad applications.^{6,7} For examples, the artificial neural network was proposed to approximate light scattering through nanoparticles and using

machine learning to simulate such optical processes was demonstrated to be orders of magnitude faster than conventional simulations.⁸ The generative adversarial network was applied to make inverse design of metasurfaces and pre-defined transmission spectra were achieved using unexpected nanostructures that beyond the intuitive design of researchers.⁹ Deep artificial neural networks have been becoming powerful tools for many applications in nanophotonics.¹⁰ Since machine learning has been demonstrated in many areas to optimize the performance of a system with multiple design parameters, it has also provided such benefits in design photonic devices (i.e. solar cells¹¹). Machine learning was even applied in the freeform optics design for significantly saving the effort in the design process¹².

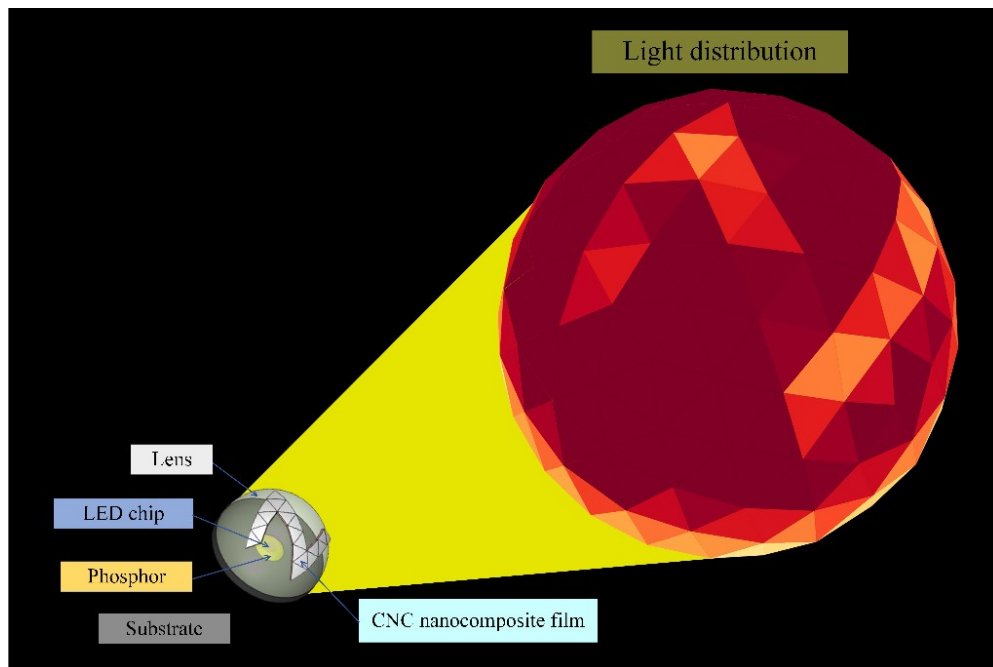


Figure 3-1: Schematic of spatial light distribution illuminated from CNC nanocomposite film coated WLED module.

Here in this work, we aim to solve the aforementioned challenges and apply scattering optics for LED lighting. Specially, we demonstrate how machine learning can be used in the inverse design of optical diffusers for WLEDs and achieve desired brightness patterns. It is well known that optical scatters on a particular location at the surface of a WLED module will diffuse light away

from this spatial direction. Thus, a patterned optical diffuser on the WLED module will produce a brightness pattern similar to the optical diffuser itself, as shown in Fig. 3-1. However, the brightness can not be completely suppressed to zero in the dark regions and the edge of the brightness pattern is not as sharp as the schematic illustrated in Fig. 3-1. In order to achieve our goals of tailoring WLED light distribution, in the first step, we altered the concentration of nanocrystals inside optical diffusers to control its optical property, so the optical scatters used in this work are not commercial optical diffusers which are typically Lambertian scatters with their light emission profiles independent on direction (angle of view). These modified optical diffusers, which are made of cellulose nanocrystal (CNC) nanocomposite films⁵ in this work, provide us some freedoms to control the percentage of light scattered to various directions, though this scattering is still symmetric in space. Then, we started to choose the pattern of CNC nanocomposite films to break the symmetry of Lambertian scatters like changing the shape of a lens surface to focus light to different directions. The selection of CNC patterns is challenging if we only use a trial and error approach. As shown in Fig. 3-2, fine adjustment of CNC patterns simply according to produced brightness patterns actually led to worse patterns through iterations, opposite to the intuition of researchers. To solve this challenge, we applied convolutional neural network (CNN) to build a machine learning model for the inverse design of CNC patterns. Finally, we used the machine learning model to build the optical diffuser (CNC patterns) and the produced brightness patterns look better than the ones made through intuitive design.

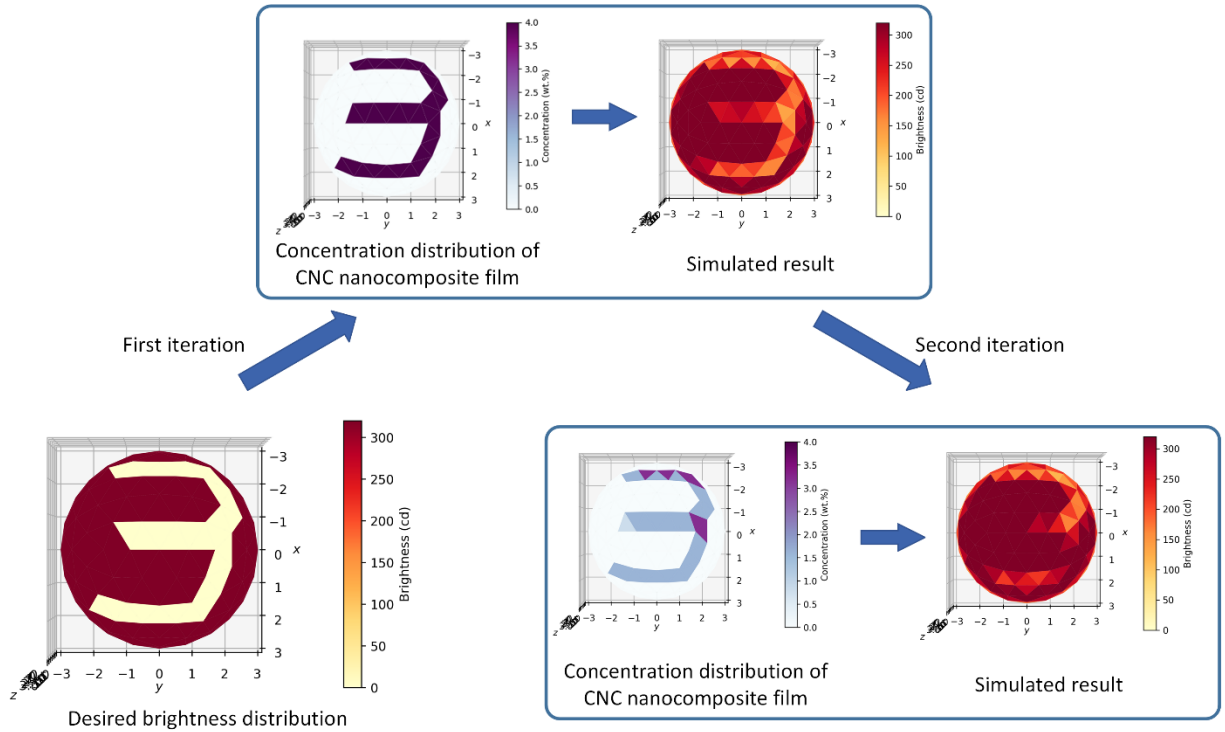


Figure 3-2: Two iterations of intuitive design “3” shape luminous flux distribution by varying the CNC nanocomposite film blocks corresponding to the previous spatial light intensity distribution.

3.2. Experimental Section

3.2.1 Optical modeling of WLED coated with CNC nanocomposite films

For general applications, we have constructed the following model of a WLED module. The size of the LED chip in WLED is $1 \times 1 \text{ mm}^2$ with a multi-layer structure which are p-GaN, multi-quantum well (MQW), n-GaN, sapphire substrate, and metal alloy film, as shown in Fig. 3-1. These layers have the thickness of 150 nm, 100 nm, 4 μm , 140 μm , and 0.1 μm , respectively. The LED chip is dispensing-coated by a phosphor-silicone and built as a spherical cap. The structure of the LED chip-coated phosphor is inside a hemisphere silicone lens with a radius of 3 mm. The optical properties and material characteristics of CNC used as an optical diffuser on a WLED module have been introduced in our previous studies.^{13–15} Commercial optical ray tracing software Zemax is used to calculate the spatial distribution of brightness based on the concentration. In the simulation, the particle size is set as 3 μm , and works of literature have shown small changes

in the size of the CNC particles, and the uniformity of the CNC dispersion had little effect on the optical properties of the nanocomposite films. The phosphor concentration is set as 0.21 g/cm³, which is fulfilled to produce white light, and its particle size is 8 μm. The two specific wavelengths applied in the simulated optical system are 454 nm and 569 nm, which can represent the blue and yellow light, respectively.

In order to straightly display the desired light distribution and construct a physical model to show the pattern of CNC nanocomposite film, we propose a new spherical triangular structure formed by regular icosahedron as the basic block, and the pattern of the CNC nanocomposite film (optical diffuser) covering the WLED module is assembled with many such blocks. As an ideal regular polyhedron, the icosahedron can produce uniform spherical triangles with the same shape by projecting onto a circumscribed sphere. Meanwhile, previous research has confirmed that the deep learning approach can perform calculations such as implementing convolution computing on the icosahedral circumscribed sphere triangle.^{16,17} In this study, considering the possibility of constructing the CNC film blocks on the WLED module and the accuracy of the simulation, we continuously divided the CNC nanocomposite film of the circumscribed hemisphere of the icosahedron twice. Initially, we cut the hemispherical CNC nanocomposite film that can cover the WLED module into a shape composed of multiple spherical triangles according to projecting the regular icosahedron to the circumscribed sphere. After that, we then selected the midpoints of each side of the triangle projected onto the sphere, divided each into 4 triangles, and repeated the dividing process. Completing the two subdivision processes and 168 triangles covering the entire hemisphere can be obtained. This number of triangles has the ability to ensure that the subsequent neural network extracts features around each block to a certain extent. Besides that, it can achieve most of the required shape design in optics representation.

3.2.2 Inverse design of CNC nanocomposite films for desired spatial distribution of LED light intensity

Based on this hemisphere shape consisting of spherical triangles, the complete intuitive approach for realizing one specific distribution of light distribution is shown in Fig. 3-3(a). For every single design object, intuitive design needs to manually assign specific concentrations of each CNC nanocomposite film block according to experiences. The simulations are then required to be finished, and one result of brightness distribution can be obtained. According to the previously simulated results, the following design can properly change several concentrations of blocks and expect a minor error between the target and the current design. Thus, after dozens/hundreds of generations, one distribution of CNC concentration can be found and used as one useful solution to realize the desired distribution of brightness. This brute force approach (solving a problem through exhaustion) is extremely time-consuming. For example, when intuitive design is used to tackle the question, one optical simulation with Zemax takes at least 1.5 hours, involving rebuilding the distribution of CNC concentrations and simulation period. For this reason, the inverse design takes a prohibitive amount of time for the iterative process, which limits the usefulness of the intuitive inverse design.

As mentioned in the introduction, one may think of a shortcut intuitive design by tweaking the CNC composite films according to previously obtained spatial distribution of light intensity. For example, the brightness distribution of one 3 shape-formed CNC nanocomposite film concentration distribution can be obtained by a simulation. The standard intuitive inverse design method is to reconstruct each block corresponding to its brightness amplitude. The CNC nanocomposite film with a concentration of 4 wt.% has been verified to realize Lambertian distribution. Thus the concentration of blocks will be set from 0 to 4 wt.% by categorizing their brightness into different ranges. The blocks showing the low and high brightness can be given concentrations such as 2 wt.% and 4 wt.%, respectively. After construction and simulation, we

found the intuitive inverse design failed to generative equally quality results as we desired because each brightness value of the block is affected by the surrounding concentrations and the exact brightness provided by the WLED module based on their position on the hemisphere space. Therefore, manual inverse design at least needs plenty of work processes to intuitively control and maintain CNC nanocomposite film concentration distribution until the results reach the target.

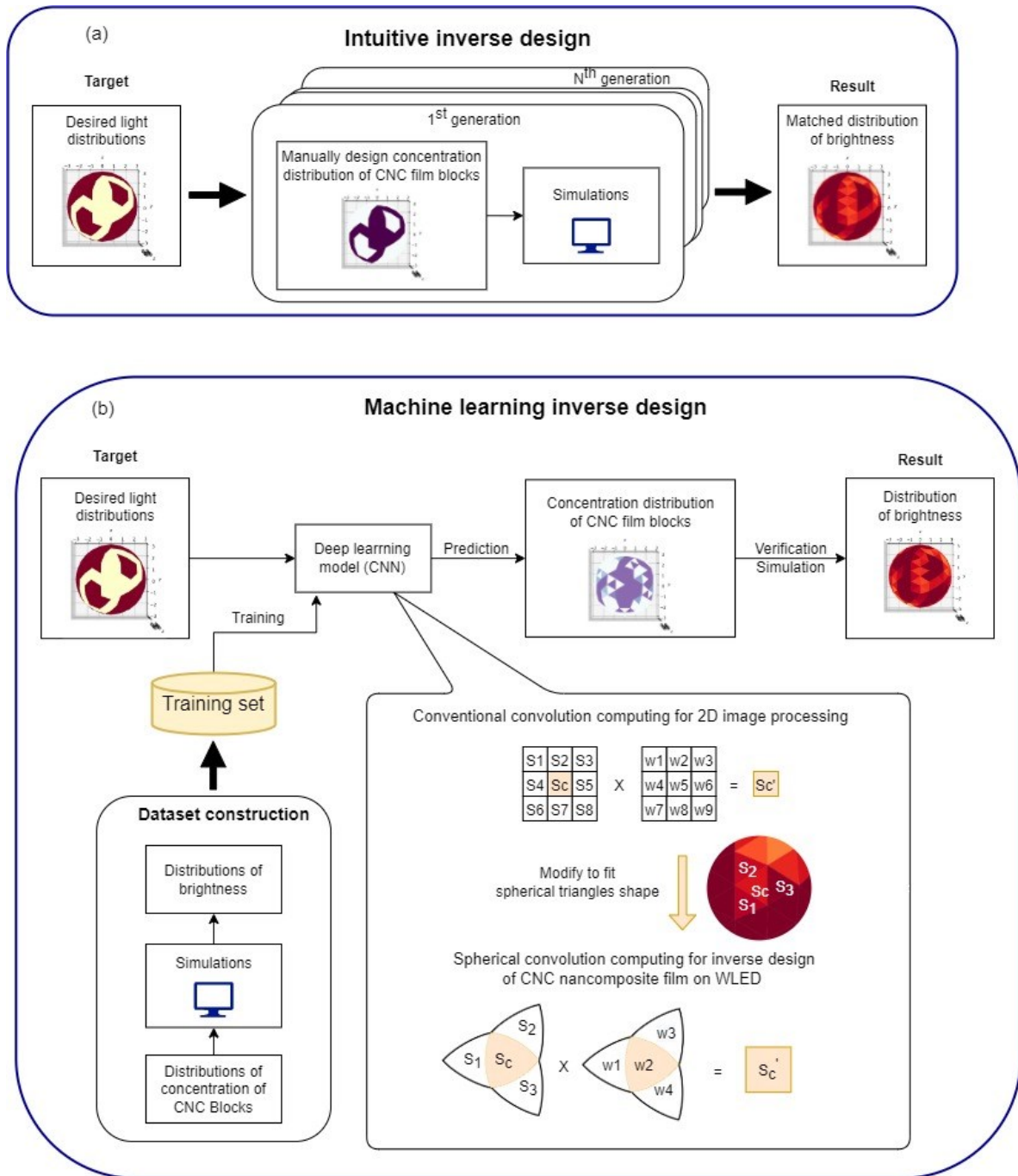


Figure 3-3: Flowchart of the entire design scheme of (a) intuitive inverse design. (b) machine learning inverse design.

To mitigate this limitation, the workflow of the deep learning approach is shown in Fig. 3-3(b). The desired distribution of brightness can be used as input, and output of the architecture is the

distribution of concentration of CNC film blocks. There are three phases in the whole inverse design process. The first phase is the construction of the dataset. As discussed above, we have constructed a convolution neural network to realize the deep learning-based optical reverse design. For conventional convolution computing, the kernel matrix commonly tackles a rectangular pixel region within images as input. Compared to conventional convolution networks, spherical convolutional computing is designed to fit the convolution calculation on the triangle blocks of the circumscribed hemisphere of the regular icosahedron. Most of the triangle blocks are adjacent to three other blocks, and the rest are near the two blocks. Therefore, a 1×4 kernel matrix ($[w_1, w_2, w_3, w_4]$) can extract the surrounding features of a certain block. In the final phase, several new user-defined light distributions are fed into the deep learning architecture as test data set. The simulation is used to verify the correctness of these predicted new patterns. Consequently, this deep learning approach can search for new solutions for the desired goals in less than a minute.

3.2.3 Training Dataset for machine learning inverse design

We constructed a dataset containing 45 sets of geometric data divided into three categories: numbers, letters, circles, and fans. The CNC blocks on the WLED module that can form the corresponding shape are then selected and set a concentration randomly chosen in the range from 1 wt.% to 4 wt.%. To receive a detailed distribution of brightness the hemisphere space, we use the same 168 spherical triangles outside the WLED module as the optical observer, and 168 sets of brightness values can be collected after simulations. After constructing the geometry of the CNC film-based optical diffuser, the distribution of brightness data is simulated using the commercial optical ray tracing software Zemax. Among them, the concentration distribution of the CNC nanocomposite film and related light brightness distribution are the input and output data, respectively.

3.3. Result and Analysis

3.1 Inverse design: model developed and evaluation

According to the description of the network structure and design process, we know that the CNN network can calculate the brightness of each block according to the light power of its surrounding blocks. Recording the connection relationship between each block is the basis for constructing a spherical convolutional network. The initial step is to index each block of the hemisphere from 1 to 168. The numbering method starts from the central triangular block containing 16 small triangle blocks and then indexes each block sequentially by layer. After completing the definition of each block, we implement a 168×168 adjacency matrix where both the index of rows and columns represent the indices of the corresponding blocks. The element set to 1 in the matrix means that the two blocks represented by its row and column numbers are adjacent or the row and column index represent the same block, while the element value of 0 demonstrates that the two blocks are non-adjacent. Involving this adjacent matrix into the neural network design, we can customize each block to only consider convolution computing with its adjacent blocks and update weights. In the meantime, as described above, the convolution kernel has four weights, resulting in the sequence problem that needs to be considered when multiplying with the data of the brightness of adjacent blocks. In other words, the adjacency list only provides the connection relationship without arranging the position in the matrix for each block. A sequence table is further constructed in which the block itself is the first element of the matrix, and the blocks at the remaining three positions are embedded in the clockwise direction of the target block. In addition, as presented above, the spatial light power detector is composed of precisely the same 168 blocks without any material doped. Before running simulations and constructing the neural network architecture, we first simulate the bare WLED module without adding any optical diffuser. By analyzing the distribution of its brightness, we found that the data of brightness received by the blocks located approximately at the bottom two layers are much smaller than that

of the blocks on the upper layer and are still decreasing layer by layer. In comparison, for the brightness distribution of the upper layer, although the brightness starts to drop from the top of the center of the model, the attenuation is small, and the brightness of the light can still be maintained at a high level. Furthermore, we performed simulations on the upper and the two lower layers with identical amounts and distributions of CNC nanocomposite films. The simulation results show that the received brightness at the lower level is relatively low, and there is no noticeable effect of dispersing light by adhering to CNC based optical diffuser. Adding CNC nanocomposite films has a strong suppression effect on decreasing the light for the blocks with high light brightness in the upper layer. Unlike general point light sources, the rectangular-shaped light source of the LED chip causes the distribution of brightness on the space hemisphere surface gradually decrease from the top layer to the bottom layer. Meanwhile, in most typical engineering practical application scenarios, the desired distribution of brightness is designed in a relatively large range based on the center of the model. From the perspective of machine learning, we compared the convolution calculations of the lower two layers and the upper layer and found that the convolution kernel has distinctly different convergence directions when tackling the two different distributions of data. Moreover, it shows a more stable and efficient convergence state when dealing with the layer convolution calculation of features of the upper layer. Therefore, according to the design requirements of optics and machine learning, we decided to remove the blocks of the bottom two layers (40 CNC nanocomposite film blocks) and only learn the blocks of the upper layer when building the neural network model to ensure the accuracy and functionality of the model.

We further modify the dataset and create an adjacency matrix with sequential relationships according to the above description. Fig. 3-4(a) shows the CNC film design of shape “3” in the data set, and the simulation result is shown in Fig. 3-4(b). Subsequently, we construct a convolutional neural network applying a dual channel with one spherical convolution in each channel. The

neural network models are implemented using PyTorch. A rectified linear unit (ReLU) activation function follows each convolution layer. For the convolution as the input layer, the 88×1 light intensity distribution matrix will be used as the input of both convolutions layers in each channel and output a matrix of the same size. The two output sets of matrices are averaged to obtain a new 88×1 intermediate layer result. In order to excite neural network architecture to learn the feature distribution of data, another dual-channel spherical convolution architecture is built after the input layer. Therefore, the following hidden layers will input the outcome matrix of the previous layer and output a result of that size. The two-pass results are then passed through an average calculation and provide an 88×1 matrix as the final result of the concentration distribution matrix. The loss equation used in this neural network architecture is the mean square error function, and the optimizer uses stochastic gradient descent. Backpropagation is performed by comparing the concentration distribution in the original dataset with predicted outputs, and then the resulting gradient updates the weights of each convolution block. After training 2000 epochs according to the original data set, the mean squared error of the neural network is 0.019 without declining, which indicates that the model has reached convergence. By using the distribution of brightness of the “3” shape in the data set as the input shown in Fig. 3-4(b), our neural network architecture can then calculate the concentration distribution, as shown in Fig. 3-4(c). After reconstructing the optical diffuser based on CNC nanocomposite film according to the new data set, the simulation provides the brightness distribution shown in Fig. 3-4(d). Based on human-eyes observations, the deep learning model can predict the concentration distribution of a new set of films with this small loss error, and the WLED module with the optical diffuser of this set of concentrations can achieve a light distribution similar to the data set. Fig. 3-4(e) compares the brightness distribution of shape “3” in the original dataset and is achievable by the concentration distribution predicted by the neural network and offers an average percentage error of 10%. The model can complete the target with high accuracy, which means that the training process of the neural network model is adequate and effective. On the other hand, the neural network model also finds a new set of

solutions for an existing light distribution result, which provides a model basis for our subsequent prediction work. By analysis, two main reasons lead to the neural network can perform excellent functionality based on only 45 sets of data sets. The first part is to remove the irreverent block that negatively influences the training process while we design the entire optical model. This preprocessing makes the model easier to fit within a relatively short training period. Secondly, using multiple convolutions in the neural network model construction can make the model more robust to the data and effectively extract the features of the hemisphere structure.

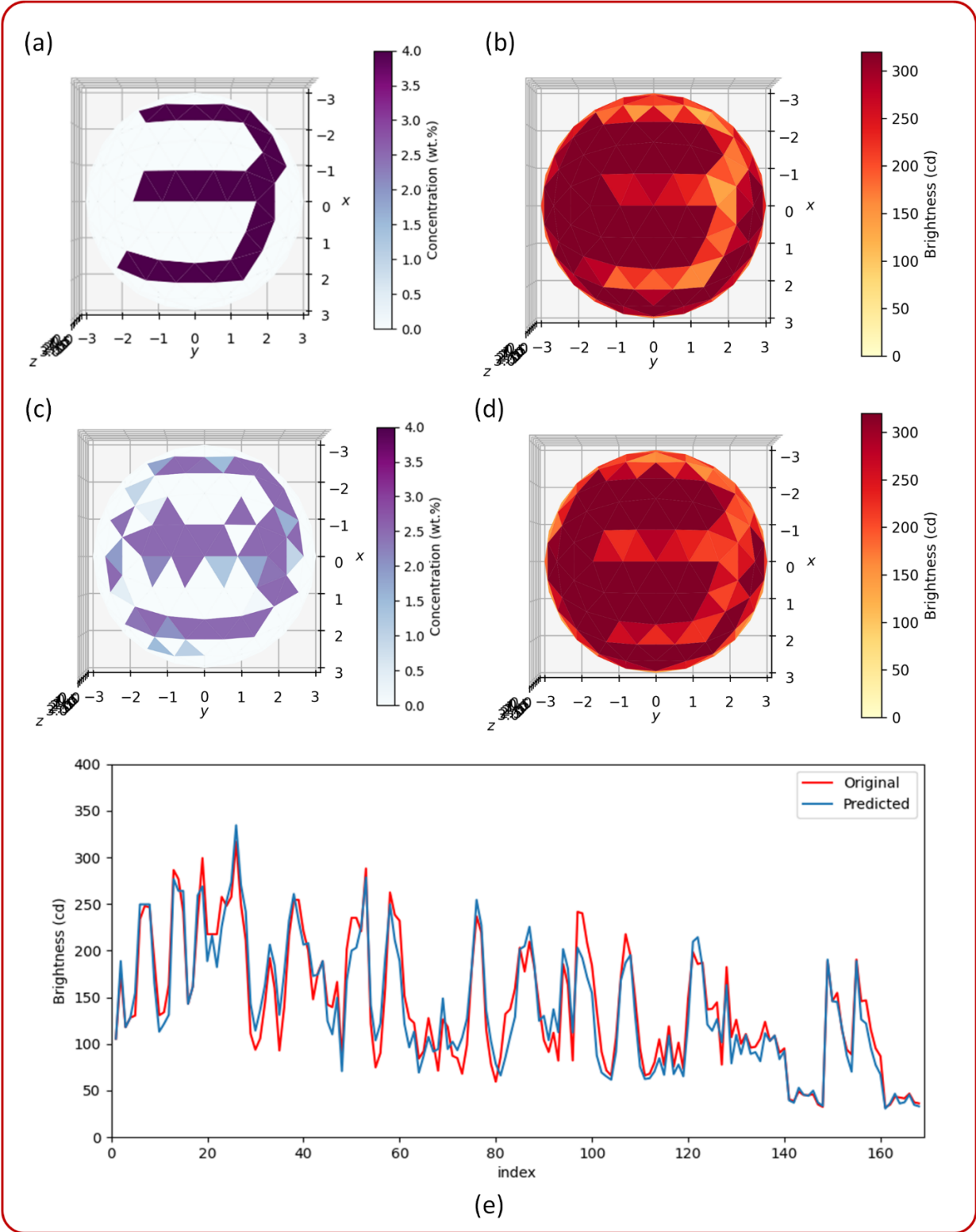


Figure 3.4: The related design and simulated results of shape “3” in both the original data set and predicted by the dee learning method. (a) CNC nanocomposite film concentration distribution in original data set. (b) Simulation

result of brightness distribution in the original data set. (c) Concentration distribution predicted by deep learning approach. (d) Verified simulation result of the brightness distribution of neural network architecture. (e) The comparison of the two brightness distributions in the line chart.

3.3.2 Inverse design for user-defined gradually changing patterns

Currently, our deep learning model can realize the reverse design of the CNC nanocomposite film concentration distribution based on the brightness distribution obtained by simulation. However, for the typical application of this optical modeling, the common scenario is to provide a manually designed light distribution, and the requirement is to find a concentration distribution of a set of CNC films that can achieve this distribution. Fig 3-5(a) shows a manually designed O-shaped light distribution with gradually varying brightness. For an intuitive design workflow, to achieve this target, we embed the high concentration of 4 wt.% in the block with the lowest brightness and then gradually fill the entire “O” shape from 4 to 0 wt.%, as shown in Fig. 3-5(b). However, after simulation, the result of this design fails to provide the expected gradually changing brightness distribution, as shown in Fig. 3-5(c). Because the light amplitude of each area is affected by at least three surrounding blocks, it is difficult to achieve the desired effect only by designing the concentration of the blocks within the target shape. Compared to the intuitive design, we directly fed the target brightness distribution into the well-trained neural network architecture, and then the model predicted a new set of concentration distributions, as shown in Fig. 3-5(d). Through simulation, this set of concentration distributions can achieve the distribution of brightness as shown in Fig. 3-5(e). Although the result provided by the deep learning model is still different from the desired target and there are certain disturbances around, machine learning distributes the appropriate concentration around each block by calculating the brightness changes around each block. Compared with intuitive design, the reverse design method of machine learning quickly achieves results that are difficult to achieve with human design.

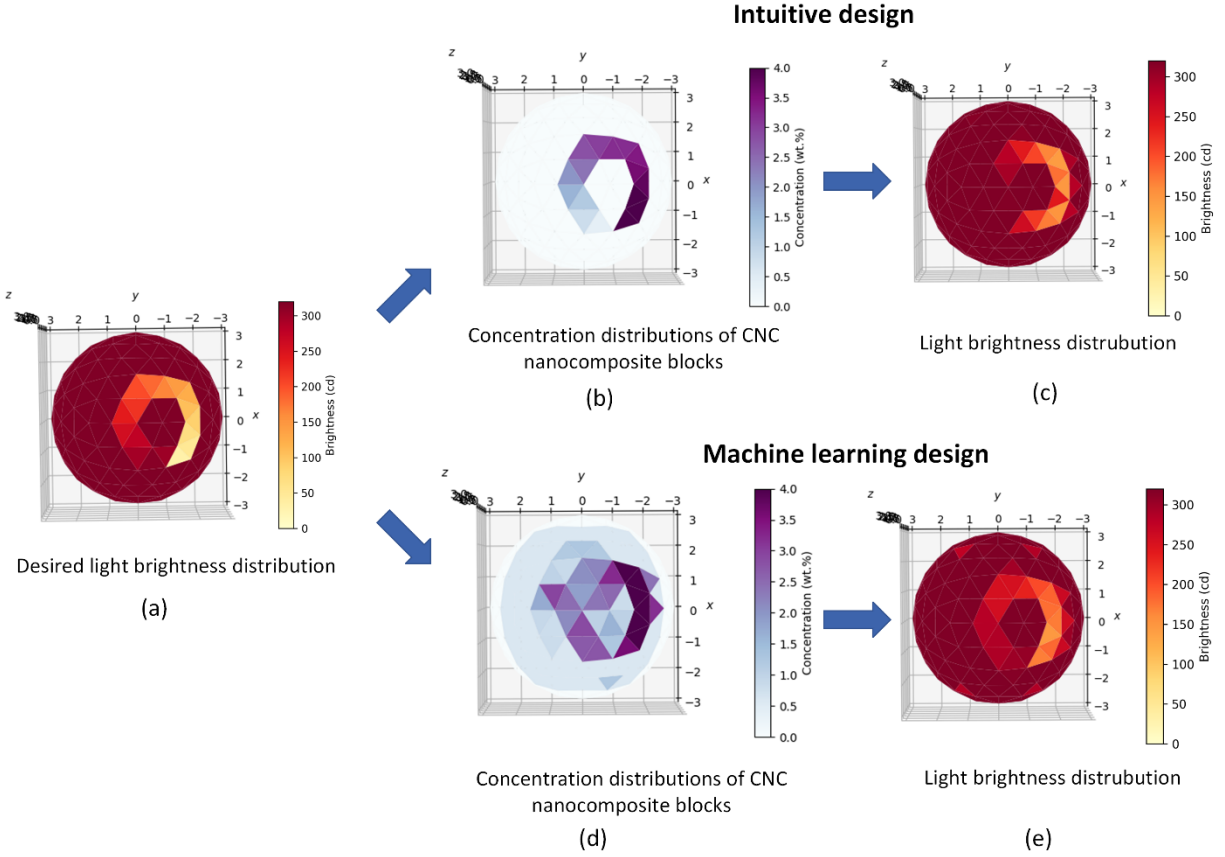


Figure 3.5: (a) The “O” shape as the desired gradually varying light distribution target. (b) The concentration distribution of CNC nanocomposite film and its (c) simulated result of brightness distribution in an intuitive design. (d) The concentration distribution of CNC nanocomposite film and its (e) simulated result of brightness distribution in machine learning design.

3.4 Conclusion

In conclusion, we have achieved to apply scattering optics for LED lighting which has never been demonstrated before. Control brightness distribution of a WLED using optical diffusers is challenging, since it is well known that optical diffusers are lack of the ability to focus light. We solved this problem by using machine learning method to reversely design the concentration distribution of nanocrystals inside the nanocomposite film. In details, we built a spherical

convolutional network to extract the relationship between the spatial brightness distribution and the distribution of spherical triangular CNC concentrations in the hemisphere nanocomposite film. The trained neural network used the brightness distribution from the original dataset as input to derive a new set of structure parameters for the optical diffuser producing the same brightness distribution compared to the original dataset. Finally, several pre-defined patterns of WLED light were realized in the trained neural network. The success of our machine learning approach to apply scattering optics for LED lighting open the door to include scattering optics in the illumination design. This work can also foster the adoption of machine learning in photonics research.

Reference

- (1) Fischer, Robert, Biljana Tadic-Galeb, and Paul Yoder. **2008**. Optical System Design. 2nd ed. New York: . <https://www.accessengineeringlibrary.com/content/book/9780071472487>
- (2) R. John Koschel, "Introduction and Terminology," in *Illumination Engineering: Design with Nonimaging Optics*, IEEE, **2013**, pp.1-30, <https://doi.org/10.1002/9781118462539.ch1>.
- (3) Falaggis, K.; Rolland, J.; Duerr, F.; Sohn, A. Freeform Optics: Introduction. *Opt Express* **2022**, *30* (4), 6450. <https://doi.org/10.1364/oe.454788>.
- (4) Bauer, A.; Schiesser, E. M.; Rolland, J. P. Starting Geometry Creation and Design Method for Freeform Optics. *Nat Commun* **2018**, *9* (1). <https://doi.org/10.1038/s41467-018-04186-9>.
- (5) Mahpeykar, S. M.; Zhao, Y.; Li, X.; Yang, Z.; Xu, Q.; Lu, Z. H.; Sargent, E. H.; Wang, X. Cellulose Nanocrystal:Polymer Hybrid Optical Diffusers for Index-Matching-Free Light Management in Optoelectronic Devices. *Adv Opt Mater* **2017**, *5* (21). <https://doi.org/10.1002/adom.201700430>.
- (6) Malkiel, I.; Mrejen, M.; Nagler, A.; Arieli, U.; Wolf, L.; Suchowski, H. Plasmonic Nanostructure Design and Characterization via Deep Learning. *Light Sci Appl* **2018**, *7* (1). <https://doi.org/10.1038/s41377-018-0060-7>.
- (7) Ma, W.; Liu, Z.; Kudyshev, Z. A.; Boltasseva, A.; Cai, W.; Liu, Y. Deep Learning for the Design of Photonic Structures. *Nature Photonics*. Nature Research February 1, **2021**, pp 77–90. <https://doi.org/10.1038/s41566-020-0685-y>.
- (8) Peurifoy, J.; Shen, Y.; Jing, L.; Yang, Y.; Cano-Renteria, F.; Delacy, B. G.; Joannopoulos, J. D.; Tegmark, M.; Soljačić, M. *Nanophotonic Particle Simulation and Inverse Design Using Artificial Neural Networks*; **2018**. <https://github.com/iguanas/ScatterNet>.
- (9) Liu, Z.; Zhu, D.; Rodrigues, S. P.; Lee, K. T.; Cai, W. Generative Model for the Inverse Design of Metasurfaces. *Nano Lett* **2018**, *18* (10), 6570–6576. <https://doi.org/10.1021/acs.nanolett.8b03171>.
- (10) Wiecha, P. R.; Muskens, O. L. Deep Learning Meets Nanophotonics: A Generalized Accurate Predictor for near Fields and Far Fields of Arbitrary 3D Nanostructures. *Nano Lett* **2020**, *20* (1), 329–338. <https://doi.org/10.1021/acs.nanolett.9b03971>.
- (11) Ripalda, J. M.; Buencuerpo, J.; García, I. Solar Cell Designs by Maximizing Energy Production Based on Machine Learning Clustering of Spectral Variations. *Nat Commun* **2018**, *9* (1). <https://doi.org/10.1038/s41467-018-07431-3>.
- (12) Zhang, B.; Jin, G.; Zhu, J. Towards Automatic Freeform Optics Design: Coarse and Fine Search of the Three-Mirror Solution Space. *Light Sci Appl* **2021**, *10* (1). <https://doi.org/10.1038/s41377-021-00510-z>.
- (13) Li, G.; Liu, Y.; Xu, Q.; Liang, H.; Wang, X. Deep Learning Enabled Inverse Design of Nanocrystal-Based Optical Diffusers for Efficient White LED Lighting. *Appl Opt* **2022**, *61* (29). <https://doi.org/10.1364/AO.471243>.

- (14) Wang, P. C.; Su, Y. K.; Lin, C. L.; Huang, G. S. Improving Performance and Reducing Amount of Phosphor Required in Packaging of White LEDs With TiO₂-Doped Silicone. *IEEE Electron Device Letters* **2014**, *35* (6), 657–659. <https://doi.org/10.1109/LED.2014.2318037>.
- (15) Xu, Q.; Meng, L.; Wang, X. Nanocrystal-Filled Polymer for Improving Angular Color Uniformity of Phosphor-Converted White LEDs. *Appl Opt* **2019**, *58* (27), 7649. <https://doi.org/10.1364/ao.58.007649>.
- (16) Cohen, T. S.; Geiger, M.; Koehler, J.; Welling, M. Spherical CNNs. **2018**.
- (17) Weyn, J. A.; Durran, D. R.; Caruana, R. Improving Data-Driven Global Weather Prediction Using Deep Convolutional Neural Networks on a Cubed Sphere. *J Adv Model Earth Syst* **2020**, *12* (9). <https://doi.org/10.1029/2020MS002109>.

Chapter 4. Conclusions and future works

4.1 Conclusions

In conclusion, we have applied machine learning to achieve the reverse design of CNC-based optical diffusers on WLED modules and improved the performance of WLEDs in this thesis work. By tuning the CNC concentration in CNC nanocomposite films, we have changed the scattering property of the CNC-based optical diffusers, and this ability of producing non-Lambertian light scatters are required to achieve the control of CCT distribution and luminous intensity (brightness) distribution. In order to solve the inverse design problem, we have constructed different neural network architectures to learn the relationship between the structural parameters of the CNC nanocomposite film adhering to a WLED module and the output performance for different illumination applications. Finally, optimized performance metrics, luminous flux and CCT in Chapter 2 and brightness distribution in Chapter 3 are accomplished. The detailed contributions in this thesis work are summarised in the following paragraphs.

In the thesis work shown in Chapter 2, we have reported the deep learning enabled inverse design of nanocrystal-based optical diffusers for efficient white LED lighting. For the first time, we demonstrated a deep learning-based inverse design approach to design optical diffusers on WLED modules for improving luminous flux and ACU simultaneously. This work opens the door to apply optical diffusers for existing WLED modules and improve the performance of existing devices on the market. To accomplish this work, the CNC nanocomposite film involving a top-coverage and one side-ring was designed to coat on the WLED module, and this design consisted of four structural parameters. The output was set to be major figures of merit of WLEDs: luminous flux and derivation of the maximum and minimum CCT values. Firstly, we designed a forward deep neural network (DNN) that could successfully predict two figures of merit with high accuracy. And then, a tandem network architecture was designed to train a reverse network that inversely

designed structural parameters. Finally, based on the reverse design results, the forward neural network was used to sample the valid data set selected from the reasonable ranges and it predicted several structure parameters for better performance.

In the thesis work shown in Chapter 3, we have achieved the demonstration to apply scattering optics for LED lighting. For the first time, we proposed a method to control brightness distribution of a WLED using optical diffusers, which are known to be lack of the ability to focus light. We achieved it by using machine learning method to reversely design the concentration distribution of the CNC nanocomposite film coating on the WLED module. Based on the geometric characteristics of the icosahedron, the CNC nanocomposite film coating on the hemisphere was divided into 168 spherical triangles. We built a spherical convolutional network to extract the relationship between the spatial brightness distribution and the distribution of spherical triangular CNC concentrations in the hemisphere. Then, the trained neural network used the brightness distribution from the original dataset as input to derive a new set of concentration distributions that achieves the exact brightness distribution. Finally, several pre-defined WLED light distribution patterns were realized in the trained neural network and it proved the success of our machine learning approach.

4.2 Future works

This thesis successfully realized the reverse design of the CNC nanocomposite film coating on the WLED module for various illumination applications by using machine learning. The neural network architecture can accurately predict the structure of CNC nanocomposite film based on the desired performances. Although our machine learning method shows excellent potential in inverse design of optical diffusers for illumination, there are still challenges that need to be addressed before commercial use. Here we propose the future works are proposed below.

4.2.1 Fabrication and experimental verification

As we mentioned above, the collection of the original data set and subsequent verifications are both based on optical simulations. Besides, the optimized structures of CNC nanocomposite films predicted from the neural network architecture are also proved to be valid through simulation using software rather than collecting the experimental results from real devices. Thus, for commercial applications, it is necessary to manufacture the actual CNC nanocomposite film on the WLED module and validate the design. The experimental verification can be first done in a research lab. If it is successful, it can be carried forward to test in practical environments.

4.2.2 Improvement of neural network architecture

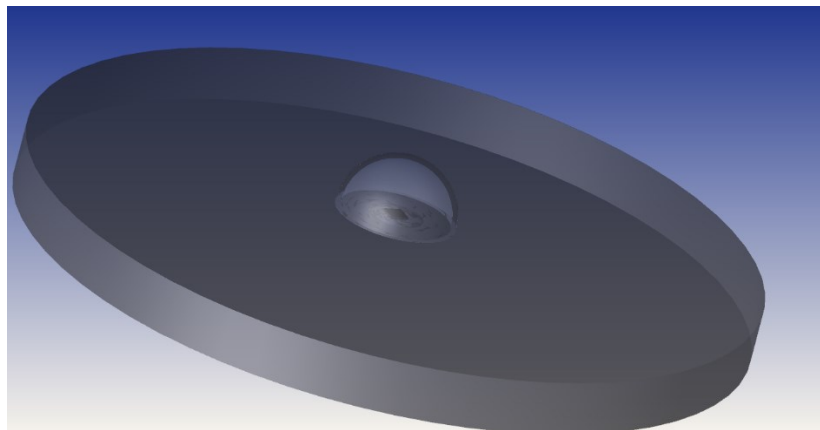
For now, our neural networks can successfully predict the results for a three-dimensional design. However, there are still two parts that can be optimized for the current models. In order to further decrease the percentage error, one utterly different network model or more complex, carefully designed neural network architecture can be built to search the relationship between the input features and output performances. Furthermore, the original data set should be enlarged to ensure more correct training and forecast more accurate results.

Appendix – Optical simulation using Zemax

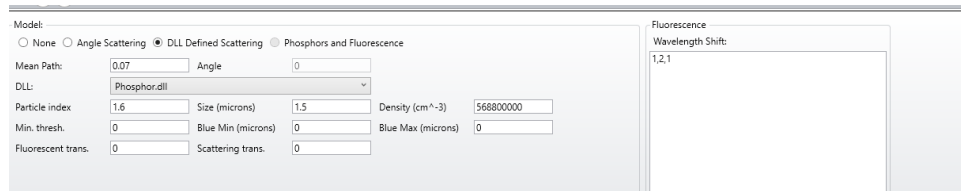
In this thesis work, the optical modeling was carried out using the commercial ray tracing software - Zemax. To build an optical model, all the parts of the model are constructed as objects in the software. By using its ray tracing function, this simulation software can provide various outputs for different demands. The thesis focused on applying CNC nanocomposite film to realize or improve the performance of the WLED module. We used the phosphor-converted WLED model to realize the white illumination, and such model involved a blue LED chip, a phosphor layer, a silicone substrate, and the coverage hemisphere (lens). The Mode used for our WLED module was based on the non-sequential. The following figure shows the object editor of the construction of this WLED module with CNC nanocomposite films in Zemax.

Object Type	Comment	Ref OI	Inside Of	X Position	Y Position	Z Position	Tilt About X	Tilt A	Tilt	Material	X1 Half Width	Y1 Half Width	Z Length
1 Standard Lens ▾	CNP film	0	0	0.000	0.000	3.000 P	0.000	0.0...	0.0..	PDMS.ZTG	-3.000	0.000	3.000
2 Standard Lens ▾		0	0	0.000	0.000	0.000	0.000	0.0...	0.0..	SILICONE.Z...	0.000	0.000	3.000
3 Standard Lens ▾	phosphor in silicone	0	-1	0.000	0.000	0.000	0.000	0.0...	0.0..	SILICONE.Z...	0.000	0.000	1.500
4 Rectangular Volume ▾	metal alloy substrate	0	-1	0.000	0.000	0.000	0.000	0.0...	0.0..		0.500	0.500	0.140
5 Rectangular Volume ▾	p-GaN	0	-2	0.000	0.000	0.140 P	0.000	0.0...	0.0..	GAN.ZTG	0.500	0.500	4.000E-03
6 Rectangular Volume ▾	MQW	-1	-3	0.000	0.000	4.000E-03 P	0.000	0.0...	0.0..	MQW.ZTG	0.500	0.500	1.000E-04
7 Rectangular Volume ▾	n-GaN	-1	-4	0.000	0.000	1.000E-04 P	0.000	0.0...	0.0..	GAN.ZTG	0.500	0.500	1.500E-04
8 Source Rectangle ▾	source in MQW	-1	-5	0.000	0.000	2.000E-04 P	0.000	0.0...	0.0..	-	0	1E+06	10.000
9 Cylinder Volume ▾	reflector	0	0	0.000	0.000	-3.000 P	0.000	0.0...	0.0..		20.000	3.000	20.000
10 Detector Polar ▾		0	0	0.000	0.000	0.000	0.000	0.0...	0.0..		80.000	150.000	20

And the NSC-shaded model of the bare WLED is shown in the following figure.



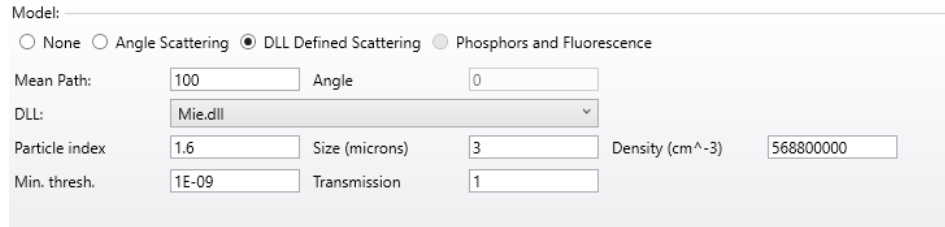
The LED chip contained five layers: p-GaN, multi-quantum well (MQW), n-GaN, a sapphire substrate, and metal alloy film. The thicknesses of each layer were 150 nm, 100 nm, 4 μm , 140 μm , and 0.1 μm , respectively. All these layers were built as rectangular volume objects in the software and their material properties and thickness were entered with appropriate values. All these parameters for this LED chip were provided from the previous literature using the Monte Carlo method and experiments to design the WLED module in Zemax that could realize the same performance as the standard WLED module. Based on multiple simulations process, we set the number of analysis rays as 1×10^6 to produce the stable and accurate simulated results. After that, a phosphor in silicone was constructed in a phosphor DLL-defined scattering model in the Zemax with all the physical properties provided by the literature. The phosphor DLL setting is shown in the following figure.



Especially since the light out of the phosphor was the yellow illumination, to describe that in the software, we used two wavelengths in the wavelength shift window of this object, which were blue and yellow light set as 454 nm and 569 nm, respectively. Additionally, there was an object type of cylinder volume below the WLED chip as a substrate. The hemisphere lens of this WLED module was built in the standard len object in the material of PDMS, and its radius was set as 3 mm. Overall, we built the complete WLED structure in the Zemax, which could be directly used in the two projects shown in this thesis work. The results from these two projects are summarized and shown in Chapter 2 and 3 of this thesis.

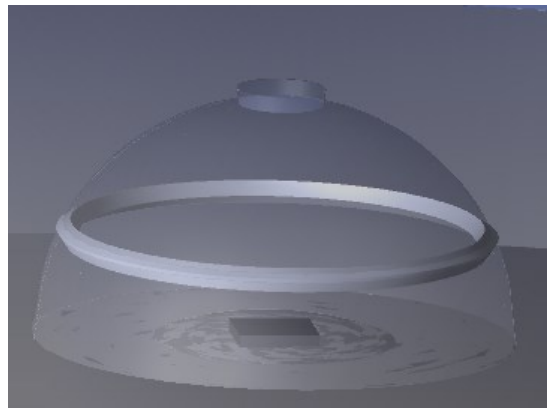
For the first project, we used a ring shape and central coverage shape of CNC nanocomposite film on the WLED module. To build two CNC nanocomposite films, we used a standard lens object

whose material was set as PDMS. Based on our previous literature, CNC nanocomposite could accomplish the Mie scattering with its particle size. Thus, we used the Mie DLL-defined scattering model within the object setting and set the corresponding material properties to make this CNC film. The specific set of material properties of CNC nanocomposite film is shown in the following figure.



Model:			
<input type="radio"/> None	<input type="radio"/> Angle Scattering	<input checked="" type="radio"/> DLL Defined Scattering	<input type="radio"/> Phosphors and Fluorescence
Mean Path:	<input type="text" value="100"/>	Angle	<input type="text" value="0"/>
DLL:	<input type="text" value="Mie.dll"/>		
Particle index	<input type="text" value="1.6"/>	Size (microns)	<input type="text" value="3"/>
		Density (cm ⁻³)	<input type="text" value="568800000"/>
Min. thresh.	<input type="text" value="1E-09"/>	Transmission	<input type="text" value="1"/>

Since the concentrations and thickness of CNC film were the varied parameters in this project, we could change the radius and density of this object to arrange different values to reflect the changes. The final step was to set an optical detector in Zemax to provide the final performance of this structure. Therefore, we added a polar detector, which can directly provide a luminous flux of the desired viewer ranges (-90° - 90°). Besides, it could also provide the tristimulus values varied with the angles, and the CCT of each angle could be directly calculated based on the diagrams. The NSC-shaded model of the WLED with two shapes of CNC nanocomposite films is shown in the following figure.



In the second project, the objects of the WLED module could be the same as in the first project. The differences were that we considered dividing the non-symmetric patterns on WLED and the whole hemisphere into 168 spherical triangles. To begin with, we constructed the hemisphere consisting of 169 spherical triangles in the Solidworks by using the multiple cutting and rotation processes, as shown in the figure below. In the construction process, we arranged the fixed thickness of 0.3 mm for each block, and the concentration of the CNC film was the only changed parameter. And other properties of CNC material could use the same values as chosen in the first project to construct the model.

After that, all the triangles were exported as IGS files from Solidworks and transferred to the internal CAD part folder in Zemax. The below figure shows the object editor of a 3-shape CNC nanocomposite film, in which each block was constructed based on the CAD object and could directly use the IGS file to assign on the WLED.

Object Type	Comment	Ref Object	Inside Of	X Position	Y Position	Z Position	Tilt About X	Tilt About Y	Tilt About Z	Material	Scale	Mode	# X-Voxels	# Y-Vox	# Z-Vox
Source Rectangle	source in MQW	-1	-5	0.000	0.000	2.000E-04	P	0.000	0.000	0.000	0	1E+06	10,000	1	0
Cylinder Volume	reflector	0	0	0.000	0.000	-3.000	P	0.000	0.000	0.000	20,000	3,000	20,000	1	0
CAD Part: STEP/IGES/SAT	1.igs	0	0	0.000	0.000	0.000	180.000	0.000	0.000		6,000		1	5	5
CAD Part: STEP/IGES/SAT	2.igs	0	0	0.000	0.000	0.000	180.000	0.000	0.000		6,000		1	5	5
CAD Part: STEP/IGES/SAT	3.igs	0	0	0.000	0.000	0.000	180.000	0.000	0.000		6,000		1	5	5
CAD Part: STEP/IGES/SAT	4.igs	0	0	0.000	0.000	0.000	180.000	0.000	0.000		6,000		1	5	5
CAD Part: STEP/IGES/SAT	5.igs	0	0	0.000	0.000	0.000	180.000	0.000	0.000		6,000		1	5	5
CAD Part: STEP/IGES/SAT	6.igs	0	0	0.000	0.000	0.000	180.000	0.000	0.000		6,000		1	5	5
CAD Part: STEP/IGES/SAT	7.igs	0	0	0.000	0.000	0.000	180.000	0.000	0.000		6,000		1	5	5
CAD Part: STEP/IGES/SAT	8.igs	0	0	0.000	0.000	0.000	180.000	0.000	0.000		6,000		1	5	5
CAD Part: STEP/IGES/SAT	9.igs	0	0	0.000	0.000	0.000	180.000	0.000	0.000		6,000		1	5	5
CAD Part: STEP/IGES/SAT	10.igs	0	0	0.000	0.000	0.000	180.000	0.000	0.000		6,000		1	5	5
CAD Part: STEP/IGES/SAT	11.igs	0	0	0.000	0.000	0.000	180.000	0.000	0.000		6,000		1	5	5
CAD Part: STEP/IGES/SAT	12.igs	0	0	0.000	0.000	0.000	180.000	0.000	0.000		6,000		1	5	5
CAD Part: STEP/IGES/SAT	13.igs	0	0	0.000	0.000	0.000	180.000	0.000	0.000		6,000		1	5	5
CAD Part: STEP/IGES/SAT	14.igs	0	0	0.000	0.000	0.000	180.000	0.000	0.000		6,000		1	5	5
CAD Part: STEP/IGES/SAT	15.igs	0	0	0.000	0.000	0.000	180.000	0.000	0.000		6,000		1	5	5
CAD Part: STEP/IGES/SAT	16.igs	0	0	0.000	0.000	0.000	180.000	0.000	0.000		6,000		1	5	5
CAD Part: STEP/IGES/SAT	17.igs	0	0	0.000	0.000	0.000	180.000	0.000	0.000		6,000		1	5	5
CAD Part: STEP/IGES/SAT	18.igs	0	0	0.000	0.000	0.000	180.000	0.000	0.000		6,000		1	5	5
CAD Part: STEP/IGES/SAT	19.igs	0	0	0.000	0.000	0.000	180.000	0.000	0.000		6,000		1	5	5
CAD Part: STEP/IGES/SAT	20.igs	0	0	0.000	0.000	0.000	180.000	0.000	0.000		6,000		1	5	5
CAD Part: STEP/IGES/SAT	21.igs	0	0	0.000	0.000	0.000	180.000	0.000	0.000		6,000		1	5	5
CAD Part: STEP/IGES/SAT	22.igs	0	0	0.000	0.000	0.000	180.000	0.000	0.000		6,000		1	5	5
CAD Part: STEP/IGES/SAT	23.igs	0	0	0.000	0.000	0.000	180.000	0.000	0.000		6,000		1	5	5
CAD Part: STEP/IGES/SAT	24.igs	0	0	0.000	0.000	0.000	180.000	0.000	0.000		6,000		1	5	5
CAD Part: STEP/IGES/SAT	25.igs	0	0	0.000	0.000	0.000	180.000	0.000	0.000		6,000		1	5	5
CAD Part: STEP/IGES/SAT	26.igs	0	0	0.000	0.000	0.000	180.000	0.000	0.000		6,000		1	5	5
CAD Part: STEP/IGES/SAT	27.igs	0	0	0.000	0.000	0.000	180.000	0.000	0.000		6,000		1	5	5
CAD Part: STEP/IGES/SAT	28.igs	0	0	0.000	0.000	0.000	180.000	0.000	0.000		6,000		1	5	5

The object properties for each block were designed by applying the same parameters as the first projects. To automatically assign the blocks and their concentration, we used the ZOS-API function of the ZEMAX and made it connected to python. With this method, all the constructions and assignments of concentrations could be solved in about 15 minutes for one design.

Furthermore, since the luminous flux was the only performance considered in this project, to collect the distribution of luminous flux in the hemisphere space, we inserted all the 168 spherical triangles in the model, all of which were constructed without setting any properties. By checking in the “object is the observer” in Zemax, these spherical triangles could work similarly to the detector polar and directly provide received luminous flux. The following figure shows the NSC-shaded model of the WLED with 3 shapes of CNC nanocomposite film.

